Inorganic Chemistry

Article

pubs.acs.org/IC

Polyoxovanadate–Alkoxide Clusters as a Redox Reservoir for Iron

Feng Li,[†] Stephanie H. Carpenter,[†] Robert F. Higgins,[‡] Mark G. Hitt,[†] William W. Brennessel,[†] Maryline G. Ferrier,[§] Samantha K. Cary,[§] Juan S. Lezama-Pacheco,[∥] Joshua T. Wright,[⊥] Benjamin W. Stein,[§] Matthew P. Shores,[‡] Michael L. Neidig,[†] Stosh A. Kozimor,[§] and Ellen M. Matson*[,†]

[†]Department of Chemistry, University of Rochester, Rochester, New York 14627, United States

[‡]Department of Chemistry, Colorado State University, Fort Collins, Colorado 80523, United States

[§]Los Alamos National Laboratory, Los Alamos, New Mexico 87545, United States

[∥]Stanford University, Stanford, California 94305, United States

[⊥]Department of Physics and CSRRI, Illinois Institute of Technology, 2101 S. Dearborn Street Chicago, Illinois 60616, United States

Supporting Information

ABSTRACT: Inspired by the multielectron redox chemistry achieved using conventional organic-based redox-active ligands, we have characterized a series of iron-functionalized polyoxovanadate–alkoxide clusters in which the metal oxide scaffold functions as a three-dimensional, electron-deficient metalloligand. Four heterometallic clusters were prepared through sequential reduction, demonstrating that the metal oxide scaffold is capable of storing up to four electrons. These reduced products were characterized by cyclic voltammetry, IR, electronic absorption, and ^{1}H NMR spectroscopies. Moreover, Mössbauer and X-ray absorption spectroscopies suggest that the redox events involve primarily the vanadium ions, while the iron atoms remained in the 3+ oxidation state throughout the redox series. In this sense, the vanadium portion of the cluster mimics a conventional organic-based redox-active ligand bound to an iron(III) ion. Magnetic coupling within the hexanuclear cluster was characterized using SQUID magnetometry. Overall, the results suggest extensive electronic delocalization between the metal centers of the cluster core. These results demonstrate the ability of electronically flexible, reducible metal oxide supports to function as redox-active reservoirs for transition-metal centers.

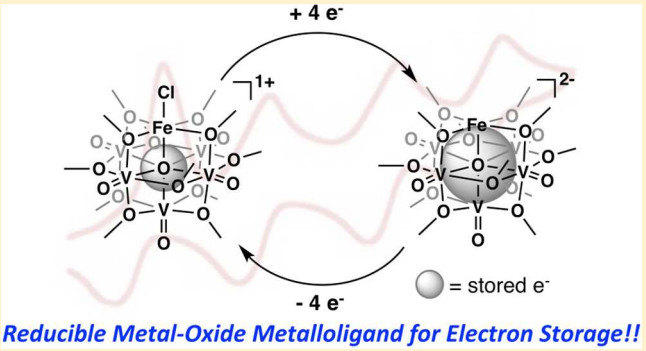

INTRODUCTION

Multielectron redox processes are often key steps in homogeneous small-molecule activation and catalytic transformations. While traditional homogeneous systems have largely featured late second- and third-row transition metals (e.g., Ru, Rh, Ir, Pd, Pt), owing to their ability to engage in two-electron processes through M^{n}/M^{n+2} redox cycling,[1−3] the scarcity of these elements renders their use costly and potentially unsustainable.[4,5] Substitution of earth-abundant, first-row transition metals offers the potential to alleviate the drawbacks associated with their precious metal congeners.

However, utilization of first-row metals has proven difficult because of the tendency of these elements to undergo single-electron redox events.[6−8]

One approach to promoting the desired noble-metal reactivity across earth-abundant elements is through the use of redox-active ligands.[9,10] These highly conjugated, organic platforms possess low-lying molecular orbitals suitable for storing electrons that can be accessed during multielectron transformations. This unique trait provides alternative access to redox chemistry, obviating the need for metal participation in the electron-transfer event. In this situation, the number of possible redox events is limited to the electron storage capacity of the redox-active ligand, as opposed to the number of accessible metal-based oxidation states. Moreover, cooperativity between the metal and redox-active ligand often enables transformations that would otherwise be inaccessible, i.e., reductive cyclization,[11,12] proton reduction,[13−16] and cross-coupling catalysis.[17,18] As a result, redox-active ligands have emerged at the forefront of discovery science in inorganic chemistry.

Despite the exciting possibilities for redox-active ligands, there do exist some limitations to these systems. There are shortcomings associated with the ligand's geometry, such as many redox-active ligands cannot sterically saturate the central metal ion. There are also limitations associated with the number of electrons that can be stored on an organic ligand.

Received: March 14, 2017
Published: May 26, 2017

DOI: 10.1021/acs.inorgchem.7b00650
Inorg. Chem. 2017, 56, 7065−7080

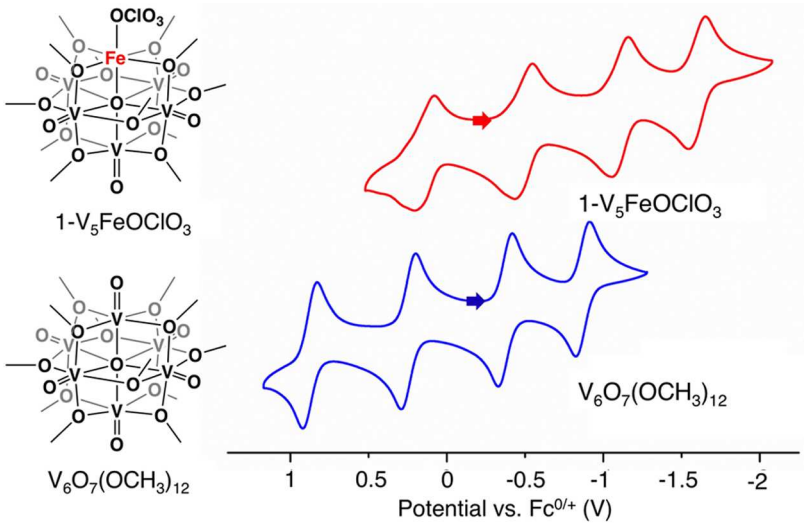

Figure 1. Cyclic voltammogram of complexes **1-V_5FeOClO$_3$** and $[V_6O_7(OCH_3)_{12}]$. The experiments were collected in DCM with $[^nBu_4N][PF_6]$ as the supporting electrolyte.

These issues present technical challenges in developing platforms for multielectron chemistry. In an attempt to overcome these obstacles, we have recently initiated investigations probing the application of metal oxide metalloligands as electron reservoirs for a first-row metal center. These alternative supports offer an opportunity to sterically saturate a heterometallic ion embedded within the cluster core, while also simultaneously providing the ability to store multiple reducing equivalents that can be used for the mediation of multielectron processes across first-row metal centers. Polyoxometalates (POMs) are a special class of molecules composed of high-valent metal oxide subunits.[19−21] Similar to the highly delocalized lowest unoccupied molecular orbitals of organic redox-active ligands, the empty d orbitals of the POM can function as sites for the storage of electron density. The redox properties and exceptional stability of these clusters have resulted in their application in photocatalysis[22−24] and homogeneous catalysis.[25−27] The goal of our research is to design POM-based metalloligands that take advantage of these steric and electronic properties, using them as redox-active reservoirs to facilitate challenging multielectron transformations.

Recently, our research group reported the synthesis of an iron-functionalized polyoxovanadate−alkoxide (FePOV−alkoxide) complex.[28] The high degree of redox flexibility reported previously for these mixed-valent vanadium oxide clusters led to the proposal that these stable frameworks could be used as redox-active scaffolds for a heterometal embedded within the Lindqvist core.[29,30] The advantage to using POV−alkoxide metalloligands as opposed to traditional organic redox-active ligands is 2-fold: (1) the robust metal oxide ligand provides a unique, three-dimensional coordination environment for the metal center and (2) these POV−alkoxide clusters potentially are capable of storing up to five reducing equivalents across the d^0 V═O moieties of the Lindqvist core (one electron at *each* oxidized vanadium ion). Furthermore, the self-assembled synthesis of these structures and their moderate air and moisture stability affords facile formation to the desired complexes.[28] Herein, we describe the synthesis and characterization of an iron-functionalized POV−alkoxide cluster, as well as members of the redox series isolated by chemical reduction and oxidation. Rigorous exploration of the electronic properties of the redox series demonstrates the ability of the reducible metal oxide scaffold to function as a redox-active metalloligand for a first-row transition-metal center.

RESULTS AND DISCUSSION

Synthesis of Reduced FePOV−Alkoxide Clusters. Recently, we reported the synthesis and characterization of an FePOV−alkoxide cluster, namely, $[V_5O_6(OCH_3)_{12}FeX]$ (**1-V_5FeX**; X = Cl, OTf, OTf = trifluoromethylsulfonate).[28] This rare example of a heterometallic polyoxovanadate−alkoxide (POV−alkoxide) cluster offers a unique opportunity to explore new approaches to the facilitation of multielectron redox chemistry with first-row metal centers. To facilitate future reactivity studies, we have optimized the reaction conditions and prepared the FePOV−alkoxide clusters using more atom- and time-efficient procedures. The monoiron perchlorate derivative, **1-V_5FeOClO$_3$**, was prepared in a manner similar to that of **1-V_5FeOTf**. Installation of the perchlorate anion ($OClO_3^-$) increased the crystallinity of the sample, allowing for facile purification and structural analysis of the product (Figures S1−S3 and Table S1). Most notably, these synthetic procedures enabled **1-V_5FeOClO$_3$** to be prepared in high purity and in sufficient quantities for subsequent characterization efforts. The cyclic voltammogram of complex **1-V_5FeOClO$_3$** revealed the rich redox chemistry of this heterometallic assembly (Figure 1 and Table 1). Similar to the previously reported **1-V_5FeOTf** complex and its homometallic hexavanadate analogue, four successive single-electron redox events were observed, suggesting the existence of five, isostructural FePOV−alkoxide clusters, differing in oxidation

Table 1. Redox Potentials Obtained from the Cyclic Voltammogram of 1-V_5FeOClO$_3$

redox process (electron distribution of metal ions)	$E_{1/2}$ (V) vs $Fc^{0/+}$ in DCM
$[V^{IV}_2V^{V}_3Fe^{III}]^{2+} + e^- \rightleftharpoons [V^{IV}_3V^{V}_2Fe^{III}]^{+}$	+0.14
$[V^{IV}_3V^{V}_2Fe^{III}]^{+} + e^- \rightleftharpoons [V^{IV}_4V^{V}Fe^{III}]$	−0.49
$[V^{IV}_4V^{V}Fe^{III}] + e^- \rightleftharpoons [V^{IV}_5Fe^{III}]$	−1.10
$[V^{IV}_5Fe^{III}] + e^- \rightleftharpoons [V^{III}V^{IV}_4Fe^{III}]$	−1.60

DOI: 10.1021/acs.inorgchem.7b00650
Inorg. Chem. 2017, 56, 7065−7080

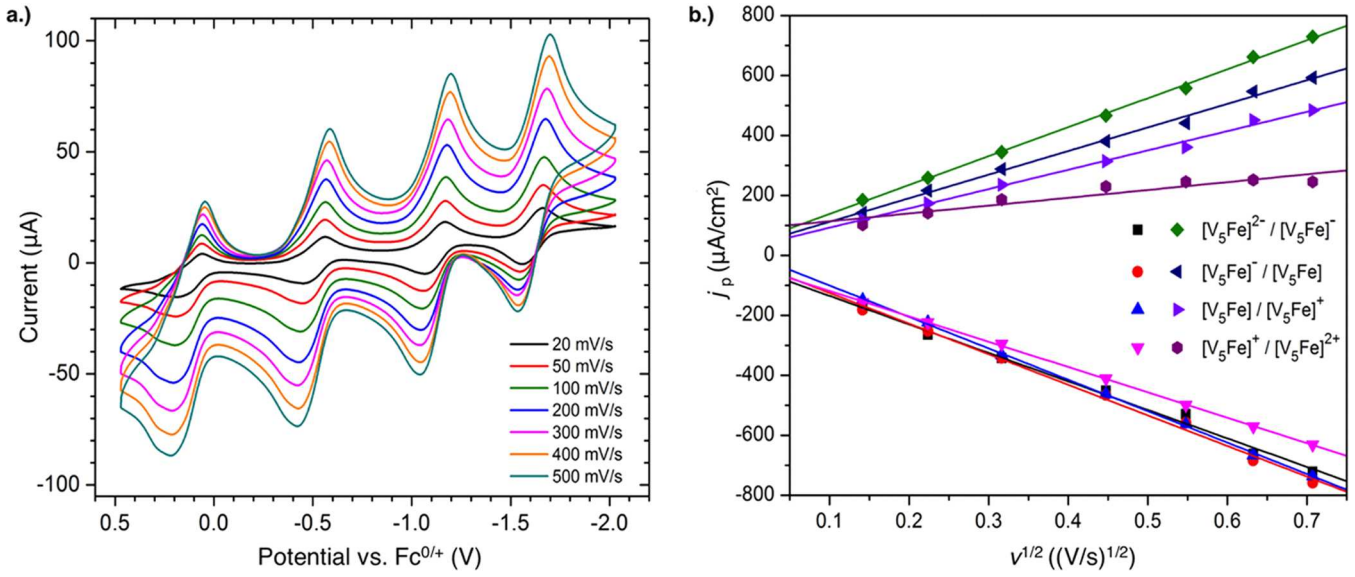

Figure 2. Electrochemical data to test the reversibility of redox couples observed for complex **1-V_5FeOClO$_3$**. (a) Cyclic voltammetry of **1-V_5FeOClO$_3$** (2 mM) taken at scan rates ranging from 20 to 500 mV s^{-1} in DCM with 0.3 M $[Bu_4N][PF_6]$ as the supporting electrolyte. (b) Plot of the current density (j_p) versus the square root of the scan rate ($\nu^{1/2}$) for complex **1-V_5FeOClO$_3$**.

Scheme 1. Sequential Chemical Reduction of 1-V_5FeOClO$_3$ to 2-V_5Fe, 3-KV_5Fe, and 4-K_2V_5Fe

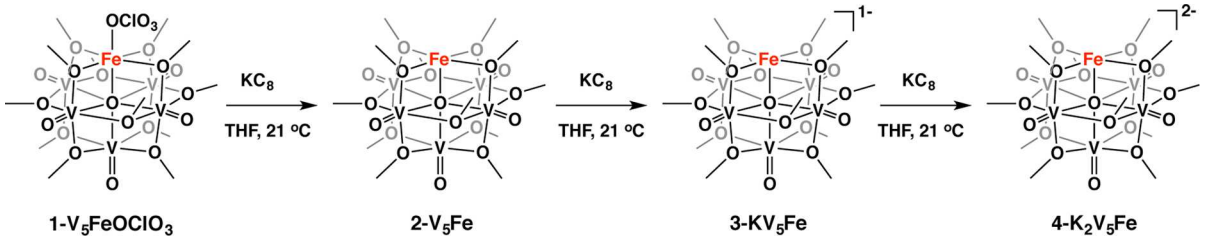

state by a single electron. The cyclic voltammograms possess redox events with peak-to-peak potentials (ΔE_p) ranging from 0.50 to 0.63 V, much larger than the theoretical Nernstian value of 0.059 V for a reversible single-electron redox event.[31]

To establish the reversibility of the redox events observed for complex **1-V_5FeOClO$_3$**, the scan rate was varied from 20 to 500 mV s^{-1} (Figure 2a). Using the Randles–Sevcik equation (1), one would expect linear behavior for a fully reversible single-electron redox event, when the current density (j_p reported in A cm^{-2}) is plotted versus the square root of the scan rate.[31]

$$J_p = 269000 n_e^{3/2} D_0^{1/2} C_0 \nu^{1/2} \quad (1)$$

In the case of eq 1, n_e is the number of electrons ($n_e = 1$), D_0 is the diffusion coefficient in cm^2 s^{-1}, C_0 is the concentration of the complex (mol L^{-1}), and ν is the voltage scan rate (V s^{-1}). The linear relationship between the square root of the scan rate and the current density is indicative of a reversible electron-transfer event for the FePOV–alkoxide complex **1-V_5FeOClO$_3$**. As observed in Figure 2b, linear fits can be observed for three stepwise single-electron reductions of **1-V_5FeOClO$_3$** located at $E_{1/2}$ values of −0.49, −1.10, and −1.60 V vs $Fc^{0/+}$. The most anodic wave, centered at +0.14 V vs $Fc^{0/+}$, deviates slightly from linearity ($R^2 = 0.87$), suggesting that the oxidation of **1-V_5FeOClO$_3$** is not a fully reversible process.

To better understand the role of the mixed-valent POV–alkoxide metalloligand in electron storage, we conducted experiments focused on isolating the reduced forms of the FePOV–alkoxide complexes. Our approach involved the stoichiometric reduction of **1-V_5FeOClO$_3$** (Scheme 1) followed by the sequential reduction of all subsequently generated products. For example, the addition of 1.1 equiv of KC_8 to complex **1-V_5FeOClO$_3$** resulted in formation of the one-electron reduction product $[V_5O_6(OCH_3)_{12}Fe]$ (**2-V_5Fe**) in good yield (70%). Analysis of the product by ^{1}H NMR and IR spectroscopies confirmed formation of the reduced compound **2-V_5Fe**, with retention of the cluster core upon reduction (Figure S4).

Treatment of **2-V_5Fe** with an additional 1 equiv of KC_8 resulted in a distinct color change from dark green to teal (Scheme 1). In previous work describing the reduction of the hexavanadate Lindqvist cluster, $[V_6O_7(OCH_3)_{12}]$, a similar color change was observed upon full reduction of the metal oxide platform, resulting in the formation of an isovalent vanadium(IV) cluster core.[29,32] Following the workup, the product $K[V_5O_6(OCH_3)_{12}Fe]$ (**3-KV$_5$Fe**) was isolated in excellent yield (91%). The ^{1}H NMR spectrum of **3-KV$_5$Fe** is composed of a single, broad resonance located at δ 23.75 (Figure S5), rendering it distinct from the multiple signals in the ^{1}H NMR spectra of complexes **1-V_5FeOClO$_3$** and **2-V_5Fe**. Subsequently, the triply reduced cluster was accessed by the addition of 1 equiv of KC_8 to **3-KV$_5$Fe**. Analysis of the product by ^{1}H NMR spectroscopy and X-ray crystallography corroborates formation of the fully reduced cluster $K_2[V_5O_6(OCH_3)_{12}Fe]$ (**4-K_2V_5Fe**) in good yield (79%; Figures 3 and S6).

DOI: 10.1021/acs.inorgchem.7b00650
Inorg. Chem. 2017, 56, 7065–7080

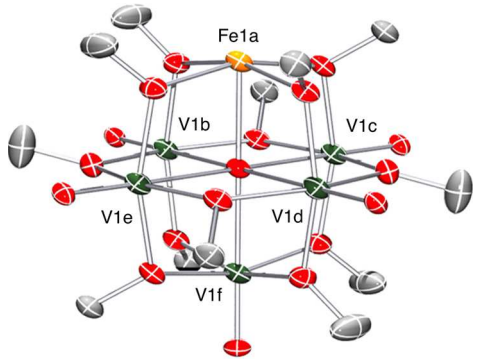

Figure 3. Molecular structure of **4-K_2VFe** shown with 50% probability ellipsoids. Hydrogen atoms and the sequestered potassium counterions have been removed for clarity.

Single crystals of **4-K_2V_5Fe** were grown via the slow diffusion of pentane into a concentrated tetrahydrofuran (THF) solution with 2 equiv of 4,7,13,16,21,24-hexaoxa-1,10-diazabicyclo[8.8.8]hexacosane (2,2,2-cryptand; Figure 3 and Table S1). Because of high symmetry, only one unique metal site was observed in the asymmetric unit, refined as $^5/_6$ V=O and $^1/_6$ Fe. As a result of the isopositional disorder, a precise assessment of the bond distances related to M−O_c and M−O_b could not be performed. The V=O_t distances [1.654(3) Å] are substantially elongated compared with those of complex **1-V_5FeOClO$_3$** (1.575 Å), consistent with the decrease in the stretching frequency noted in the IR spectra of the two clusters (Table 4 vide infra). This observation suggests an overall decrease in the oxidation state of the vanadium ions of the POV−alkoxide metalloligand. Despite the isopositional disorder of the vanadium and iron ions, the average M−O_c distance reveals an expansion of the cluster core upon reduction [the average M−O_c distance in **1-V_5FeOClO$_3$**, 2.280 Å, is less than that in **4-K_2V_5Fe**, 2.3040(6) Å]. Similar cluster expansions have been noted in the hexavanadate series: as the Lindqvist core accepts the electron density, the structure expands to accommodate the additional reducing equivalents.[29] Likewise, Harris and Betley recently reported a series of mixed-valent cyanide-ligated hexairon clusters that display an analogous trend.[33] The volume of the [Fe_6] cluster core incrementally increases upon a reduction of the system.

In addition to being accessible via successive single-electron reductions, the doubly and triply reduced clusters can be formed directly by the reduction of **1-V_5FeOClO$_3$** with 2.0 or 3.0 equiv of KC_8, respectively (Scheme 2). ^{1}H NMR and IR spectroscopies confirmed generation of the corresponding reduced complexes, albeit in lower yields (**3-KV_5Fe**, 65%; **4-K_2V_5Fe**, 55%). We have also demonstrated that reduced clusters can be oxidized back to their parent molecules via the stoichiometric addition of AgX salts (X = OTf, ClO_4). The oxidation of reduced derivatives suggests that the stored electron density can be accessed to facilitate redox transformations relevant to small-molecule activation under appropriate conditions.

Although single crystals for X-ray diffraction of **2-V_5Fe** and **3-KV_5Fe** have proven to be exceptionally difficult to obtain, the Fe K-edge extended X-ray fine structure (EXAFS) results confirmed that the identities of these compounds are best described as illustrated in Scheme 1. The solid-state $k^3\chi(k)$ EXAFS spectra experimentally obtained at room temperature from **1-V_5FeOClO$_3$**, **2-V_5Fe**, **3-KV_5Fe**, and **4-K_2V_5Fe** were

Scheme 2. Stoichiometric Multielectron Reduction and Oxidation of FePOV−Alkoxide Clusters

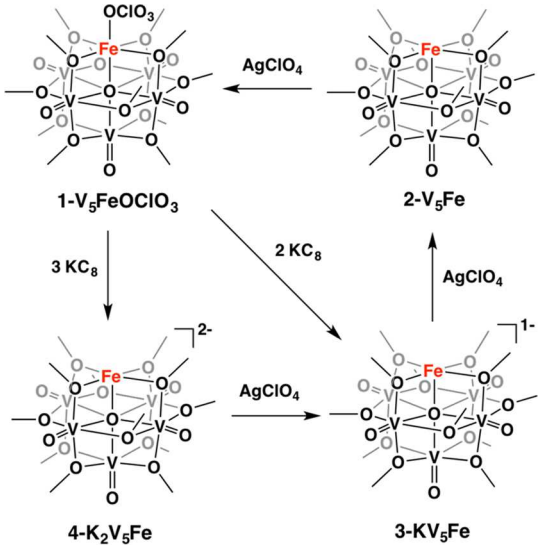

nearly superimposable (Figure 4a). Before the data were modeled, expected (FEFF8[34]) EXAFS spectra were calculated using atomic coordinates obtained from single-crystal X-ray diffraction data collected for complexes **1-V_5FeOClO$_3$** and **4-K_2V_5Fe**. These atomic coordinates from the crystal structures were used as an initial guess for the **2-V_5Fe** and **3-KV_5Fe** EXAFS models. EXAFS data were analyzed by fixing the coordination numbers based on the formulation in Scheme 1 and allowing the amplitude reduction factor (S_0^2), bond lengths (R), and Debye−Waller factors (σ^2) to converge to reasonable values. In all cases, high-quality fits with low residual factors and reduced χ^2 values were obtained (Figure 4b). The EXAFS results are summarized in Table 2, and an interpretation for all four spectra is presented (Figure 4c). Collectively, the EXAFS results confirmed that the structures of complexes **2-V_5Fe** and **3-KV_5Fe** were very similar to that of **1-V_5FeOClO$_3$** and **4-K_2V_5Fe**. However, the data were not of sufficient quality to distinguish subtle structural changes that likely accompany the redox reactions that systematically transform **1-V_5FeOClO$_3$** to **2-V_5Fe**, **3-KV_5Fe**, and **4-K_2V_5Fe** (e.g., cluster-core expansion upon reduction).

Spectroscopic Analysis of Reduced FePOV−Alkoxide Clusters. *Mössbauer and X-ray Absorption Near-Edge Spectroscopic (XANES) Studies.* With the entire series of reduced FePOV−alkoxide clusters in hand, we sought to characterize the electronic structure of these heterometallic clusters. To this end, we sought to more rigorously define the oxidation state of the unique iron center within the series of sequentially reduced FePOV−alkoxide clusters via Mössbauer and X-ray absorption (XAS) spectroscopies. The 5 K Mössbauer spectrum of **1-V_5FeOClO$_3$** was found to contain two different iron components (see Figure 5 and Table 3 for all Mössbauer spectra and parameters): a major iron species with δ = 0.52 mm s^{-1} and ΔE_Q = 1.32 mm s^{-1} (62% of iron) and a minor species with δ = 0.54 mm s^{-1} and ΔE_Q = 0.80 mm s^{-1} (38% of iron). The observed Mössbauer parameters for both components fall within the typical range for high-spin iron(III) in a tetragonal coordination environment.[35]

To justify the presence of at least two chemically distinct iron centers within the analytically pure sample of **1-V_5FeOClO$_3$**, we considered the weak coordination of the perchlorate

DOI: 10.1021/acs.inorgchem.7b00650
Inorg. Chem. 2017, 56, 7065−7080

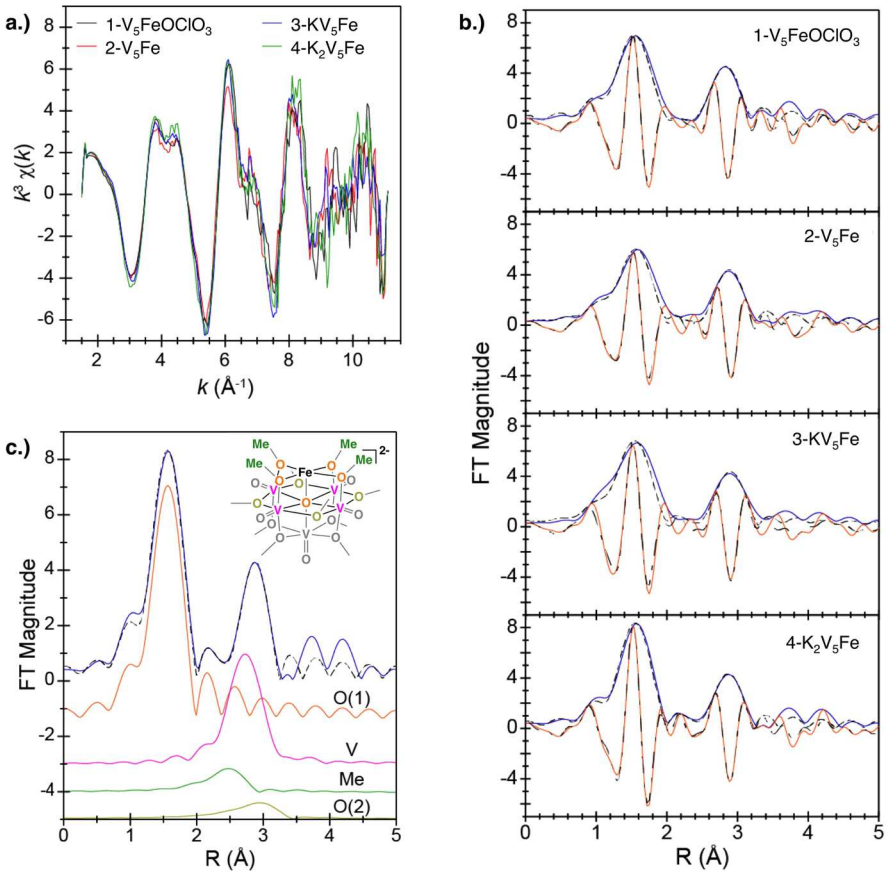

Figure 4. (a) Room temperature solid-state Fe K-edge EXAFS function $k^3\chi(k)$ from **1-V_5FeOClO$_3$**, **2-V_5Fe**, **3-KV_5Fe**, and **4-K_2V_5Fe**. (b) Fourier transform of k^3-weighted EXAFS spectra from **1-V_5FeOClO$_3$**, **2-V_5Fe**, **3-KV_5Fe**, and **4-K_2V_5Fe** shown as the blue trace, with its real part presented as the orange trace. Fits to the data have been provided as dashed black traces. (c) Interpretation of the Fourier transform of k^3-weighted EXAFS spectra from **4-K_2V_5Fe** (blue trace) overlaid on the fit to the data (dashed black traces) and contributions from oxygen (orange trace), carbon (green trace), vanadium (pink trace), and a second oxygen (olive trace) paths.

Table 2. Comparison of the EXAFS Structural Metrics from 1-V_5FeOClO$_3$, 2-V_5Fe, 3-KV_5Fe, and 4-K_2V_5Fe

compound	ΔE_0 (eV)	S_0^2	Fe−O1	O1-σ^2	Fe−Me	Me-σ^2	Fe−V	V-σ^2	Fe−O2	O2
1-V_5FeOClO$_3$	5.3 ± 1.4	0.7(1)	1.99(1)	0.009(2)	2.95(4)	0.002(4)	3.16(2)	**0.005(2)**		
2-V_5Fe	6.7 ± 2.0	0.8(2)	2.00(2)	0.024(3)	2.97(4)	0.002(4)	3.20(2)	0.006(2)		
3-KV_5Fe	5.1 ± 4.2	0.9(4)	1.99(3)	0.033(5)	3.00(13)	0.010(30)	3.21(5)	0.010(11)	3.52(12)	0.007(25)
4-K_2V_5Fe	6.0 ± 1.1	0.7(8)	1.99(1)	0.002(1)	3.01(5)	0.010(12)	3.198(3)	0.008(3)	3.54(2)	0.014(18)

counterion. Low-temperature crystallography data of **1-V_5FeOClO$_3$** revealed a neutral cluster featuring a six-coordinate iron center in which the perchlorate ion was bound to iron in an η^1 fashion through an oxygen atom (Figure S1). In contrast, electrospray ionization mass spectrometry (ESI-MS; positive mode) data suggested that **1-V_5FeOClO$_3$** behaves as an ionic compound, featuring a cationic cluster with a five-coordinate iron center, and an outer-sphere perchlorate anion (m/z 778.93; Figure S3). The conflicting spectroscopic analyses suggest that the existence of two unique electronic environments for iron in complex **1-V_5FeOClO$_3$** is the result of the hemilability of the perchlorate anion. To confirm this hypothesis, we synthesized a rigorously six-coordinate derivative of the original FePOV−alkoxide cluster. The addition of an excess of AgOCN to a crude mixture of V_5FeBr results in the formation of complex **1-V_5FeOCN** in good yield (68%), as confirmed by ^{1}H NMR and and IR spectroscopies (Figures S8 and S9, respectively). ESI-MS (positive mode) revealed that **1-V_5FeOCN** stays intact in solution during ionization (m/z 820.87), suggesting that the OCN^- moiety is consistently bound to a six-coordinate iron center (Figure S10). The Mössbauer parameters for **1-V_5FeOCN** (δ = 0.49 mm s^{-1} and ΔE_Q = 0.79 mm s^{-1}) are very similar to the minor component found in the spectrum of **1-V_5FeOClO$_3$** (Table 3). As such, the unique iron species identified in the Mössbauer spectrum of **1-V_5FeOClO$_3$** represent two different coordination environments of iron(III), a minor six-coordinate component with $OClO_3^-$ ligation, and a major five-coordinate component. In our previous publication, we suggested that **1-V_5FeX** (X = Cl, OTf, $OClO_3$) has two possible charge distributions, $[V^{IV}{}_3V^{V}{}_2Fe^{III}]^+$ or $[V^{IV}{}_2V^{V}{}_3Fe^{II}]^+$.[28] Given the unambiguous results from Mössbauer spectroscopy, we can now definitively assign the cluster-core charge distribution of **1-V_5FeX** as $[V^{IV}{}_3V^{V}{}_2Fe^{III}]^+$.

Upon reduction to **2-V_5Fe**, a single new iron species is observed by Mössbauer with δ = 0.51 mm s^{-1} and ΔE_Q = 0.89 mm s^{-1}. The observed parameters are consistent with **2-V_5Fe** retaining a high-spin iron(III) center (Table 3). Analogous

DOI: 10.1021/acs.inorgchem.7b00650
Inorg. Chem. 2017, 56, 7065−7080

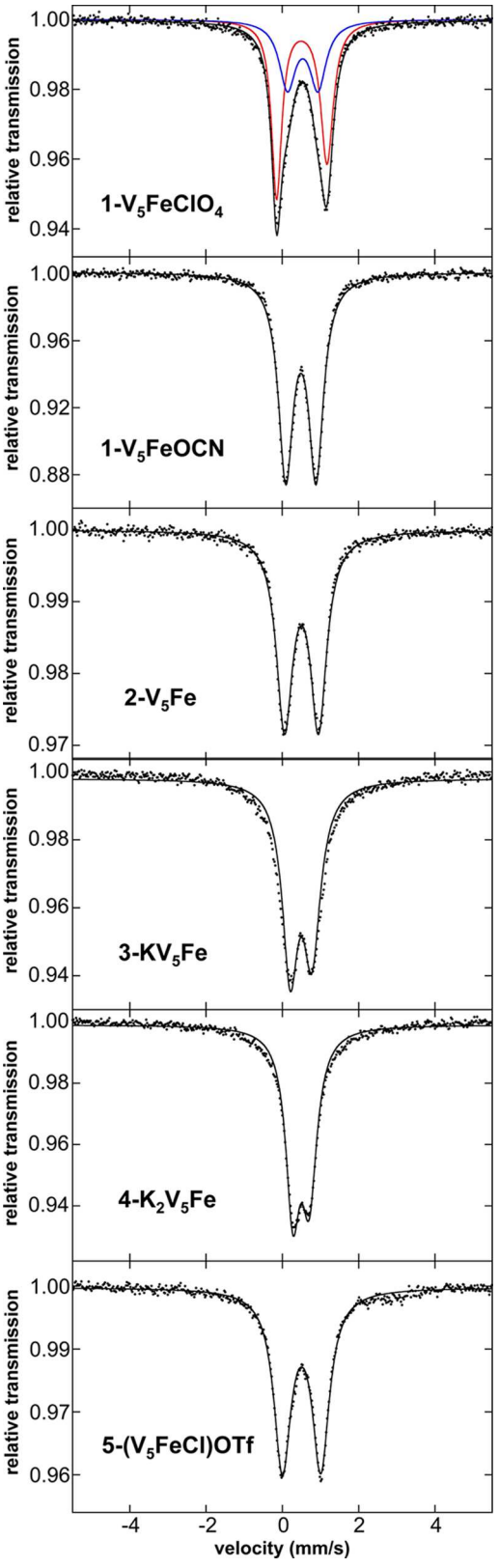

Figure 5. 5 K Mössbauer spectra of FePOV−alkoxide clusters. For each spectrum, the data (dots) and fit (solid line) are given. The Mössbauer fit parameters for each spectrum are given in Table 3. Note that for **1-V_5FeOClO$_3$** two components were required for the best fit because of the line shapes of the absorption features.

results are observed for **3-KV_5Fe** and **4-K_2V_5Fe** (Table 3), with Mössbauer parameters for both compounds consistent with high-spin iron(III) in a weak ligand field. Thus, Mössbauer spectroscopy supports the assignment of high-spin iron(III) centers across the redox series of FePOV−alkoxide clusters, suggesting that the reduction of the cluster does not involve the addition of a localized electron to the heterometal center to generate an iron(II) ion. Instead, the results indicate that the POV−alkoxide metalloligand may be involved in facilitating delocalized reduction events across the cluster core.

Table 3. ^{57}Fe Mössbauer Spectroscopic Parameters of FePOV−Alkoxide Clusters Collected at 5 K

compound	δ (mm s^{-1})	ΔE_Q (mm s^{-1})
1-V_5FeOClO$_3$	0.52	1.32[a]
	0.54	0.80[b]
1-V_5FeOCN	0.49	0.79
2-V_5Fe	0.51	0.89
3-KV_5Fe	0.49	0.57
4-K_2V_5Fe	0.49	0.43
5-V_5FeCl$^+$	0.50	1.01

[a]62% of total iron. [b]38% of total iron.

To confirm our interpretation of the Mössbauer results, XAS was employed. Comparisons of the background-subtracted and normalized Fe K-edge XANES results for **1-V_5FeOClO$_3$**, **2-V_5Fe**, **3-KV_5Fe**, and **4-K_2V_5Fe** were consistent with the interpretation of the Mössbauer data discussed above. The XANES spectra of these four analytes were nearly superimposable (Figure S11). They were dominated by two weak preedge features (~7112.9 and 7114.2 eV) that emerged at the onset of an intense absorption peak near 7133 eV (Figure 6). It is established that the low-intensity preedge features are an intimate reflection of iron's chemical environment (e.g., coordination number, geometry, oxidation state, d-orbital splitting) resulting from Fe 1s → 3d electronic transitions.[36,37] Although formally forbidden, these transitions gain intensity through allowed electric quadrupole transitions as well as from mixing between 3d and 4p orbitals, for which Fe 1s → 4p transitions are dipole-allowed.

A comparison with well-defined, five-coordinate ferrous, [Fe^{II}(MeCN)(TMC)](BF$_4$)$_2$ (TMC = 1,4,8,11-tetramethyl-1,4,8,11-tetraazacyclotetradecane), and ferric, Fe^{III}(salen)Cl [salen = *N*,*N*′-bis(salicylidene)ethylenediamine], standards reveals that the iron atoms in **1-V_5FeOClO$_3$**, **2-V_5Fe**, **3-KV_5Fe**, and **4-K_2V_5Fe** are best described as being in the 3+ oxidation state (Figures 6 and S11).[38] For example, the two preedge features for each analyte were at an average energy of ~7113.5 eV (Figure S11). These values were higher in energy than the preedge peak energies from the [Fe^{II}(MeCN)TMC](BF$_4$)$_2$ (7111.5 and 7113.8 eV; mean 7112.6 eV) standard and similar to the 7.112.8 and 7114.0 eV features from Fe^{III}(salen)Cl (mean = 7113.4 eV; Table S2). The excellent energy agreement between our measurements and the previously characterized standards enabled us to compare the average preedge peak energies from **1-V_5FeOClO$_3$**, **2-V_5Fe**, **3-KV_5Fe**, and **4-K_2V_5Fe** with those from compounds previously reported by Solomon et al. (Figure S12).[38] Despite wide variation in the coordination numbers and geometries for the Solomon data set, comparisons of **1-V_5FeOClO$_3$**, **2-V_5Fe**, **3-KV_5Fe**, and **4-K_2V_5Fe** to geometrically analogous species lend further validation in our assessment that our analytes contain iron(III) centers.

Mössbauer and XAS analysis of compounds **1-V_5FeOClO$_3$**, **2-V_5Fe**, **3-KV_5Fe**, and **4-K_2V_5Fe** agree that the iron(III)

DOI: 10.1021/acs.inorgchem.7b00650
Inorg. Chem. 2017, 56, 7065−7080

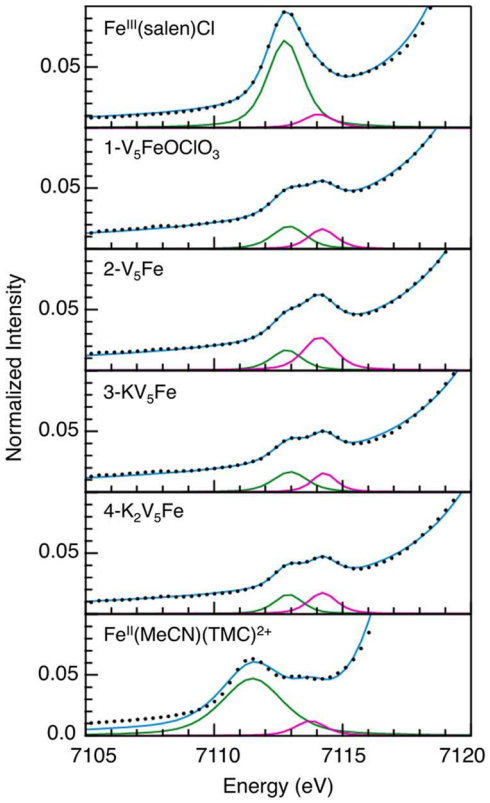

Figure 6. Comparison of the Fe K-edge XAS experimental data (•) obtained from the Fe^{III}(salen)Cl and Fe^{II}(MeCN)(TMC)$(BF_4)_2$ standards with those from the **1-V_5FeOClO$_3$**, **2-V_5Fe**, **3KV_5Fe**, and **4K_2V_5Fe** analytes. The preedge pseudo-Voigt functions (green and pink) used to generate the deconvoluted spectra (blue trace) have been included.

oxidation state is retained upon reduction of the cluster core. The extensive electronic flexibility of the POV−alkoxide framework presents a metalloligand platform capable of storing three reducing equivalents for the iron center, supporting the cluster over four redox states. This capability contrasts with the majority of organic, redox-active ligand platforms, few of which have been demonstrated as capable of storing this degree of electron density for first-row metal centers.[39−42]

IR and Electronic Absorption Spectroscopic Characterization of Reduced FePOV−Alkoxide Clusters. With an understanding of the oxidation state of ferric ions throughout the series of reduced complexes (**1-V_5FeOClO$_3$**, **2-V_5Fe**, **3-KV_5Fe**, and **4-K_2V_5Fe**), we sought to elucidate the corresponding electronic changes across the POV−alkoxide metalloligand. It is well-established that IR and electronic absorption spectroscopies can provide a deeper perspective into the bonding and electronic structure of Lindqvist POV−alkoxide clusters, $[V_6O_7(OR)_{12}]^n$ (R = CH_3, CH_2CH_3; n = 2+, 1+, 0, 1−, 2−)[29,30,43] Of particular interest is the use of these spectroscopic techniques to characterize the degree of reduction across the metal oxide scaffold.

Similar to their hexavanadate analogues, the IR spectra of complexes **1-V_5FeOClO$_3$**, **2-V_5Fe**, **3-KV_5Fe**, and **4-K_2V_5Fe** reveal two strong, broad absorption bands, corresponding to the O_b−CH_3 (O_b = bridging oxygen; 1000−1050 cm^{-1}) and V═O_t (O_t = terminal oxo; 935−985 cm^{-1}) stretching modes of the cluster (Figure 7a and Table 4).[30,44] As discussed in the case of the $[V_6O_7(OR)_{12}]^{n+}$ clusters, the large half-widths of

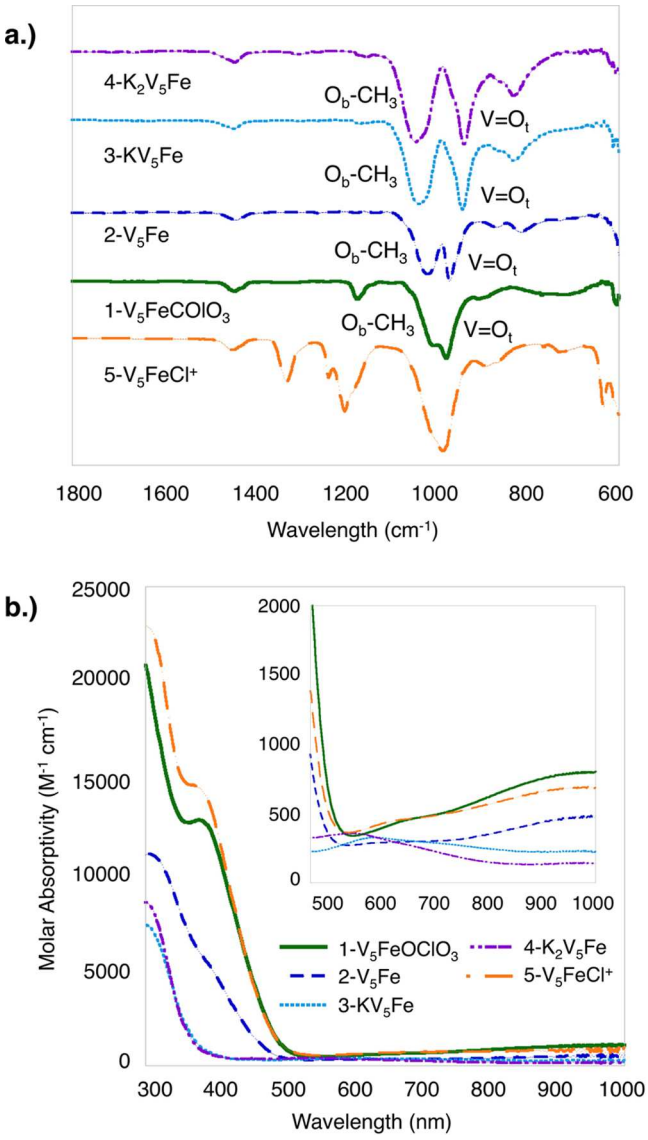

Figure 7. Spectroscopic characterization of redox isomers of FePOV−alkoxide complexes: (a) IR spectrum; (b) electronic absorption spectrum collected in THF at 21 °C. The inset shows the low-energy region of the spectrum to more clearly illustrate IVCT bands.

Table 4. IR Data for Complexes 1-V_5FeOClO$_3$, 2-V_5Fe, 3-KV_5Fe, and 4-K_2V_5Fe

compound	ν(C−H) (cm^{-1})	ν(O_b−CH_3) (cm^{-1})	ν(V═O_t) (cm^{-1})
1-V_5FeOClO$_3$	2926, 2820	1007	979
2-V_5Fe	2920, 2816	1018	972
3-KV_5Fe	2916, 2812	1038	943
4-K_2V_5Fe	2895, 2808	1047	939

these bands likely result from overlap between multiple features with similar energies.[30] Indeed, the pseudo-C_{4v} symmetry of the FePOV−alkoxide clusters should result in multiple bands for both V═O_t and O_b−CH_3 moieties. Additionally, the observed broadening of these IR bands has been associated with coalescence that occurs as a result of the coupling of geometric changes of metal−oxygen bond lengths with multimetallic electron-transfer events.[30,45] As such, the presence of single, broad bands for ν(V═O_t) and ν(O_b−CH_3) of the FePOV−

DOI: 10.1021/acs.inorgchem.7b00650
Inorg. Chem. 2017, 56, 7065−7080

alkxoide complexes suggests a substantial degree of electronic delocalization across the cluster core.

In the IR spectra of the series of reduced FePOV−alkoxide clusters, features corresponding to the $\nu(V{=}O_t)$ asymmetric stretching frequency enable the qualitative assessment of the collective oxidation states of the vanadium ions composing the metalloligand. As sequential one-electron reductions of the FePOV−alkoxide complexes are performed, $\nu(V{=}O_t)$ decreases, indicating a decrease in the average energy of the $V{=}O_t$ bond. This observation is consistent with the reduction of a vanadium ion within the POV−alkoxide metalloligand. In contrast, as electrons are added to the FePOV−alkoxide cluster, the energy of $\nu(O_b{-}CH_3)$ increases. It was established previously that the $O_b{-}CH_3$ stretching frequencies are sensitive to the degree of the overall electron density of the core.[30] With greater electron density available to the bridging oxygen atoms, the availability of electrons for interaction with the carbon center increases. This suggests an increased negative partial charge surrounding the bridging oxygen atoms, as a result of the increased d-electron count of the FePOV−alkoxide core.[30]

The pattern of changes in the IR spectra upon sequential reduction of the FePOV−alkoxide complexes further suggests that the single electron added to the system is delocalized over the cluster core, as opposed to being localized on an isolated vanadium atom or the heterometallic iron center. Importantly, $\nu(V{=}O_t)$ and $\nu(O_b{-}CH_3)$ are extremely sensitive to the electronic structure of the FePOV−alkoxide complex, offering two convenient spectroscopic handles by which analysis of the reduction reactions can be accomplished. Of particular note are the large changes in the $V{=}O_t$ and $O_b{-}CH_3$ frequencies observed upon the reduction of **2-V_5Fe** to **3-KV_5Fe**. These dramatic changes are a result of moving from a mixed-valent vanadium(V)/vanadium(IV) POV−alkoxide cluster to a homovalent vanadium(IV) structure. This spectroscopic information, coupled with analysis by cyclic voltammetry, indicates that the cluster is able to undergo several vanadium oxide based reduction events, confirming the generation of new stable reduced derivatives.

In a similar capacity, electronic absorption spectra of POV−alkoxide clusters have proven to be reliable for qualitative assessment of the distribution of oxidation states of vanadium ions within the Lindqvist core.[30,43] In the case of the FePOV−alkoxide clusters, two distinctive absorptions are assigned to intervalence charge-transfer (IVCT) bands between vanadium(IV) and vanadium(V) centers (Figure 7b). These features have been reported for both heterometallic and homometallic POV−alkoxide clusters and indicate a large degree of electronic delocalization within the cluster core.[28,43] The first band, located at lower energies (~980 nm), is commonly found in mixed-valent POMs.[46,47] This feature has been identified by Hartl and co-workers in the case of the homometallic $[V_6O_7(OCH_3)_{12}]$ clusters as a $d_{xy}(V^{IV}) \rightarrow d_{xy}(V^{V})$ excitation between two unique vanadium ions.[43] In the same study, the authors identify the IVCT band at higher energies (~370 nm) as a $d_{xy}(V^{IV}) \rightarrow d_{x^2-y^2}(V^{V})$ transition. The difference in energies between the two IVCT absorptions resembles that of the energy associated with the ligand-field transition for the homovalent Lindqvist clusters, justifying the discrepancy between energies of these charge-transfer events.[43]

From the existence of the two IVCT bands in the electronic absorption spectra of complexes **1-V_5FeOClO$_3$** and **2-V_5Fe**, we are able to confirm the mixed-valent electronic configuration vanadium ions within the POV−alkoxide scaffold. The overall decrease in the intensity of the IVCT bands in the spectrum of **2-V_5Fe** compared to that of **1-V_5FeOClO$_3$** suggests a change in the electronic properties of the metalloligand. A reduction of the additional vanadyl moiety in the cluster decreases the statistical probability of electron transfer between vanadium(IV) and vanadium(V) centers, resulting in the lower molar absorptivities of the IVCT bands for complex **2-V_5Fe**. Analogous observations were made for the neutral, homometallic $[V_6O_7(OCH_3)_{12}]$ ($V^{IV}{}_4V^{V}{}_2$), where features associated with IVCT events were significantly weakened upon reduction to $[V_6O_7(OCH_3)_{12}]^-$ ($V^{IV}{}_5V^{V}$).[43] This substantiates the previously discussed Mössbauer and XANES results and confirms that the reduction can be assigned to the delocalized POV−alkoxide metalloligand as opposed to the iron center. As such, the charge distributions for complexes **1-V_5FeOClO$_3$** and **2-V_5Fe** can be assigned as $[V^{IV}{}_3V^{V}{}_2Fe^{III}]^+$ and $[V^{IV}{}_4V^{V}Fe^{III}]$, respectively.

Analysis of the doubly reduced complex, **3-KV_5Fe**, by electronic absorption spectroscopy reveals the loss of IVCT bands, suggesting formation of the homovalent POV−alkoxide cluster via reduction of the final vanadium(V) ion. A weak absorption is observed at 590 nm (ε = 330 M^{-1} cm^{-1}), analogous to a feature in the spectrum of $[V^{IV}{}_6O_7(OCH_3)_{12}]^{2-}$ ($V^{IV}{}_6$) assigned as a $d_{xy}(V^{IV}) \rightarrow d_{x^2-y^2}(V^{IV})$ forbidden excitation.[48] The observation of the formation of a homovalent V^{IV} POV−alkoxide scaffold results in the designation of the site of the second reduction to the metalloligand. This is consistent with the retention in the oxidation state of the iron ion, as determined by Mössbauer and XAS spectroscopies. We thus assign the charge distribution of the metal centers in **3-KV_5Fe** as $[V^{IV}{}_5Fe^{III}]^-$.

Considering the invariant oxidation state of the iron center throughout the redox series (vide infra), the third reduction of the FePOV−alkoxide clusters **4-K_2V_5Fe** must primarily involve vanadium atoms. This could be realized by selectively reducing a single vanadium(IV) atom to a localized vanadium(III) ion. Alternatively, reduction could involve a metal orbital delocalized across the metal oxide cluster. In either case, reduction of the POV−alkoxide metalloligand results in a proposed charge distribution for the fully reduced cluster, **4-K_2V_5Fe**, of $[V^{III}V^{IV}{}_4Fe^{III}]^{2-}$. Analysis of the electronic absorption spectrum of complex **4-K_2V_5Fe** revealed features comparable to that of **3-KV_5Fe** in the visible region. Notably, the signature IVCT bands of complexes **1-V_5FeOClO$_3$** and **2-V_5Fe** are not present, indicating, as expected, a lack of V^V d^0 ions within the cluster core. The band associated with the forbidden $d_{xy}(V^{IV}) \rightarrow d_{x^2-y^2}(V^{IV})$ excitation has shifted from 590 nm in complex **3-KV_5Fe** to 548 nm (ε = 360 M^{-1} cm^{-1}) in **4-K_2V_5Fe**, suggesting an increase in the energy of this transition consistent with a reduction of the cluster core. Coupled with the changes noted in the IR spectrum of **4-K_2V_5Fe**, spectroscopic evidence supports the hypothesis that the final reduction occurs across the POV−alkoxide metalloligand, resulting in a charge distribution of $[V^{III}V^{IV}{}_4Fe^{III}]^{2-}$. This is in contrast to the hexavanadate system, which cannot be reduced beyond $[V^{IV}{}_6O_7(OCH_3)_{12}]^{2-}$.[29] Complex **4-$K_2V_5$Fe** represents the first example of a Lindqvist POV−alkoxide cluster containing a $[V^{III}{=}O]$ moiety. The only other known examples of a hexavanadate cluster containing vanadium(III) ions is $[(V^{III}Cl)_6O(MeC(CH_2O)_3O_4]$, where all the vanadyl groups are replaced by $[V^{III}Cl]^{2+}$,[49] and (cat)-$V_6O_6(OCH_3)_8$(calix)(CH_3OH) (cat = Et_4N^+, NH_4^+, pyridi-

DOI: 10.1021/acs.inorgchem.7b00650
Inorg. Chem. 2017, 56, 7065−7080

nium, Et_3NH^+; calix = *p-tert*-butylcalix[4]arene), which contains a $V^{III}OCH_3$ moiety.[50]

Magnetic Property Analysis of FePOV–Alkoxide Clusters. To further probe the electronic structure of the heterometallic core, magnetic susceptibility and magnetization analyses were performed for the series of sequentially reduced FePOV–alkoxide clusters. Previous work has demonstrated that homometallic mixed-valent vanadium clusters show complicated magnetic properties. For example, Zubieta and coworkers have characterized mixed-valent and isovalent hexanuclear POV–alkoxide clusters that show apparent antiferromagnetic interactions, as evidenced by a negative Weiss constant (Θ) obtained through analysis of high-temperature χ_M^{-1} versus T data.[51,52] Notably, the isovalent vanadium(IV) derivatives are reported to show long-range antiferromagnetic ordering. Likewise, Daniel and Hartl reported that the methoxide-bridged homometallic POV–alkoxide clusters have analogous thermal dependencies of magnetic susceptibilities.[43] These magnetic properties are associated with geometric spin frustration for the series of mixed-valent ($V^{IV}_5V^V$) and isovalent (V^{IV}_6) clusters.

In an effort to contextualize the magnetic properties of complexes **1**–**4**, we draw a direct comparison of the FePOV–alkoxide clusters to their homometallic, hexanuclear vanadium counterparts.[43,51,52] Magnetic susceptibility products ($\chi_M T$) for complexes **1-V_5FeOClO$_3$**, **2-V_5Fe**, **3-KV_5Fe**, and **4-K_2V_5Fe** are presented in Figure 8. The room temperature $\chi_M T$ value for

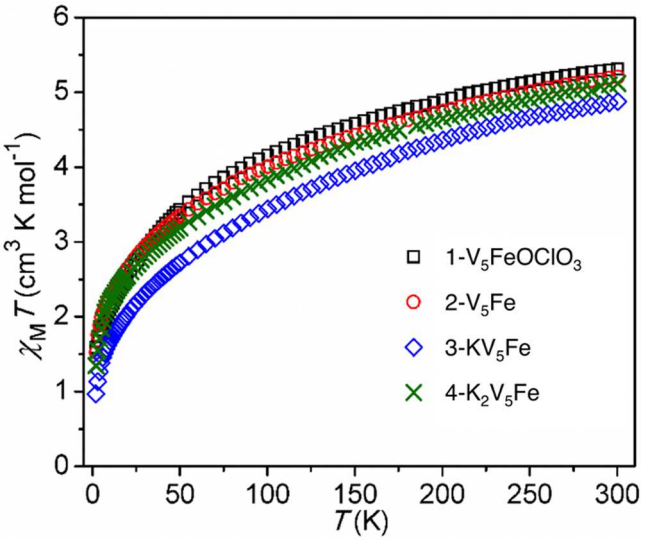

Figure 8. Temperature dependence of the magnetic susceptibility for complexes **1-V_5FeOClO$_3$**, **2-V_5Fe**, **3-KV_5Fe**, and **4-K_2V_5Fe**, collected at applied fields of 1000 Oe.

complexes **1-V_5FeOClO$_3$** (5.31 cm^3 K mol^{-1}), **2-V_5Fe** (5.21 cm^3 K mol^{-1}), **3-KV_5Fe** (4.88 cm^3 K mol^{-1}), and **4-K_2V_5Fe** (4.21 cm^3 K mol^{-1}) are slightly lower than the expected spin-only value, assuming no coupling between iron(III) and vanadium(IV/III) ions. The magnetic susceptibility values are far too large to implicate a low-spin iron(III) center, thus confirming the assignment of high-spin iron(III) ($S = {}^5/_2$) ions in all four compounds in the redox series. This observation is consistent with the results from Mössbauer experiments (vide supra). Interestingly, the room temperature magnetic susceptibility value *decreases* as the complex is reduced from **1-V_5FeOClO$_3$** to **3-KV_5Fe** and then increases slightly upon further reduction to **4-K_2V_5Fe** (Table 5). In a weakly coupled regime, one would expect $\chi_M T$ values to increase with each

Table 5. Selected Magnetic Values for Complexes 1–4

compound	$\chi_M T$ at 2 K (cm^3 K mol^{-1})	$\chi_M T$ at 300 K (cm^3 K mol^{-1})	θ (K)	M at 1.8 K and 50 kOe (μ_B)
1-V_5FeOClO$_3$	1.59	5.31	−60	2.42
2-V_5Fe	1.52	5.21	−67	2.49
3-KV_5Fe	0.97	4.88	−93	1.85
4-K_2V_5Fe	1.35	5.12	−70	2.41

added electron because diamagnetic vanadium(V) centers are sequentially reduced to doublet vanadium(IV) ions. The absence of this hypothesized behavior is consistent with increased antiferromagnetic interactions from **1-V_5FeOClO$_3$** to **3-KV_5Fe** that manifest at room temperature. It is important to note that the FePOV–alkoxide complexes do not show long-range magnetic ordering, as determined from the lack of inflection points in the χ_M versus T plots (Figure S15). This unique trait of the heterometallic cluster complexes confirms that the magnetic interactions are primarily intramolecular in nature.

For all compounds measured, $\chi_M T$ values decrease in a monotonic fashion as the temperature is lowered until ∼150 K. At lower temperatures, the decrease becomes more pronounced, reaching susceptibility values of 0.97–1.59 cm^3 K mol^{-1} at 2 K (Table 5). We note that **3-KV_5Fe** shows slightly lower $\chi_M T$ values across all temperatures. The thermal dependencies of the $\chi_M T$ values for the series of reduced FePOV–alkoxide clusters do not match those expected for a spin-state change of the iron(III) center. Instead, the large decrease in the $\chi_M T$ values indicates significant antiferromagnetic interactions between the iron(III) and vanadium(IV) ions. Specifically, a comparison of the thermal behavior of **3-KV_5Fe** with Daniel's previously reported hexanuclear vanadium(IV) analogue reveals that the iron(III) ion is not a spectator that can simply be subtracted electronically from the systems (Figures S18 and S19).

Further evidence for a delocalized electronic structure for the FePOV–alkoxide clusters rests in the analyses of plots of χ_M^{-1} versus T (Figure S16), which display linearity at high temperatures. Similar observations have been interpreted as net antiferromagnetic interactions (negative Θ) in related hexavanadium complexes.[43,51,52] Consistent with the "Θ" values reported for all-vanadium analogues (Table S3), the "Θ" values for complexes **1-V_5FeOClO$_3$**, **2-V_5Fe**, **3-KV_5Fe**, and **4-K_2V_5Fe** appear to track with the number of vanadium(IV) ions present in the FePOV–alkoxide cluster (Table 5). Strictly speaking, such an interpretation is inadequate because it assumes Curie paramagnetism with no intramolecular exchange-coupling interactions. Despite this fact, fit values are included for a comparison with previously performed analyses. Upon the introduction of the electron density via reduction, more vanadium centers possess singly occupied (local) d_{xy} orbitals, resulting in an increase in the magnitude of the intramolecular antiferromagnetic exchange (larger Θ values). This observation is noted for all four FePOV–alkoxide compounds measured, suggesting extensive antiferromagnetic coupling across the heterometallic cluster core.

Notably, compound **4-K_2V_5Fe** has a formal charge distribution of $[V^{III}V^{IV}_4Fe^{III}]$. A POV–alkoxide cluster possessing a vanadium(III) ion has not been magnetically

DOI: 10.1021/acs.inorgchem.7b00650
Inorg. Chem. 2017, 56, 7065–7080

characterized in a hexanuclear POV cluster previously. The vanadium(IIII) ion is expected to have singly occupied local d_{xz} and d_{yz} orbitals: spins in these orbitals have the proper symmetries to engage in ferromagnetic superexchange coupling through the oxo ligand if the vanadium(III) ion is in the equatorial plane with respect to the iron(III) ion. In addition, the removal of an electron from a d_{xy}-type orbital may be expected to decrease the magnitude of geometric frustration in V_3 and/or V_2Fe triangular plaquettes. Both explanations would lead to a less negative Θ value for complex **4-K_2V_5Fe**, which is observed experimentally. These analyses of the magnetic behavior of this compound at variable temperatures support the presence of a vanadium(III) ion within the cluster core.

If we consider the magnetization experiments, the values for all characterized complexes do not show saturation at fields up to 50 kOe (Figure S17). This observation gives evidence to these complexes possessing substantial electronic delocalization across the cluster core, consistent with their classification as a Robin and Day class II mixed-valent system.[53] Previously characterized octanuclear iron clusters have also been characterized as class II mixed-valent species and did not display saturation of magnetization until much larger fields (~100 kOe).[54−59] This observation is likely caused by excited-state mixing into the ground state, impeding saturation of magnetization.

The magnetic susceptibility analyses of complexes **1-$V_5FeOClO_3$**, **2-V_5Fe**, **3-KV_5Fe**, and **4-K_2V_5Fe** indicate that their magnetic properties are unlike the previously published hexanuclear POV clusters.[43] Interpretation of the magnetic data in hand suggests that the electronic structure of these clusters is most appropriately defined as class II mixed-valent compounds.[53] We are further investigating the distinct role that the iron(III) ion plays in the magnetic properties of these clusters and will report these findings in due course.

*Oxidation of **1-V_5FeX**.* Spectroscopic characterization of complexes **1**−**4** establishes a static iron(III) oxidation state for the heterometal of the FePOV−alkoxide clusters. As the complex is sequentially reduced, electrons are stored across the POV−alkoxide alkoxide scaffold, without a change of the oxidation state of iron. To complete the redox series, oxidation of complex **1-V_5FeX** (X = $OClO_3^-$, OTf^-) was attempted. The addition of a 0.33 equiv of WCl_6 results in the formation of $[V_5O_6(OCH_3)_{12}FeCl]^+$ (5-V_5FeCl^+) in moderate yield (43%; Scheme 3). The synthesis of the oxidized species was confirmed

Scheme 3. Oxidation of 1-V_5FeOTf

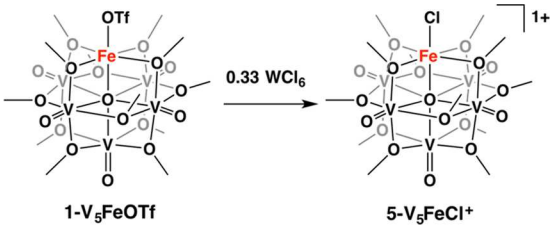

by ^1H NMR spectroscopy (δ 23.98 and 12.47; Figure S20) and ESI-MS (positive mode; *m*/*z* 814.22 (100), 815.93 (27); V_5FeCl^+; Figure S21). Given the low yield of **5-V_5FeCl^+**, partial decomposition is thought to occur during oxidation of the cluster core. Cluster degradation was confirmed via observation of the formation of the monomeric V^V precursor, $VO(OCH_3)_3$, as detected by ^1H NMR spectroscopy. Additional evidence for partial cluster decomposition following oxidation was noted in the isolated crystalline product; structural analysis via X-ray crystallography revealed the formation of **5-V_5FeCl^+**, with the counterion identified as $FeCl_4^-$ (Figure 9 and Table S1; *d*(Fe−Cl)($FeCl_4^-$) = 2.161(4)−2.244(2) Å[60,61] and *d*(Fe−Cl)-($FeCl_4^{2-}$) = 2.282(2)−2.3547 Å[62−64]).[65] These observations are consistent with the quasi-reversibility of the oxidation event ($E_{1/2}$ = +0.14 V vs $Fc^{0/+}$) in the cyclic voltammogram of **1-$V_5FeOClO_3$** (Figure 2).

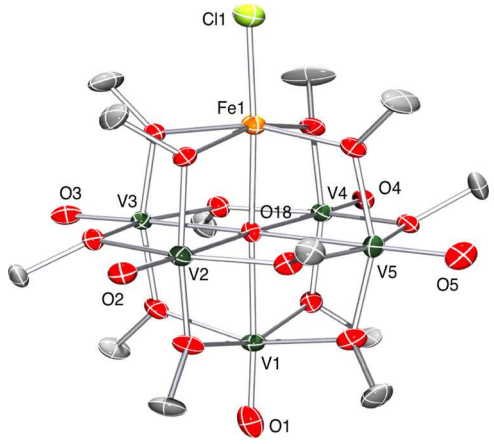

Figure 9. Molecular structure of **5-V_5FeCl^+** shown with 50% probability ellipsoids. The $[FeCl_4]^-$ counterion and solvent molecule has been removed for clarity.

Conducting the oxidation of **1-V_5FeOTf** at lower temperatures and over shorter reaction times led to the minimization of cluster degradation and the isolation of complex **5-V_5FeCl^+** with a trilfate counterion, as confirmed by elemental analysis. Spectroscopic characterization of complex **5-[V_5FeCl]OTf** revealed changes in the electronic structure of the metal oxide platform, suggesting that a delocalized oxidation event occurs across the metalloligand platform. The IR spectrum of **5-V_5FeCl^+** exhibited an increase in the energy of the V═O_t stretching frequency (986 cm^{-1}), supporting oxidation of the POV−alkoxide scaffold (Figure 7a). The electronic absorption spectrum of **5-[V_5FeCl]$^+$** is similar to that of **1-$V_5FeOClO_3$**, with IVCT bands at 988 nm (ε = 691 M^{-1} cm^{-1}) and 370 nm (ε = 14600 M^{-1} cm^{-1}) (Figure 7b). The molar absorptivities of the IVCT bands are similar in magnitude to that of **1-$V_5FeOClO_3$**. This is due to two possible charge-transfer events between vanadium(IV) and vanadium(V) within the cluster core of each compound. An additional strong absorption band is observed at 302 nm (ε = 22930 M^{-1} cm^{-1}), assigned to the Cl: → Fe^{III} ligand-to-metal charge transfer.

To confirm oxidation of the metalloligand as opposed to the heterometal, Mössbauer spectroscopy of complex **5-[V_5FeCl]-OTf** was performed. The 5 K Mössbauer spectrum of **5-V_5FeCl^+** was fit to contain a single iron species (Figure 5, vide supra) with δ = 0.50 mm s^{-1} and ΔE_Q = 1.01 mm s^{-1}. The observed Mössbauer parameters for complex **5-V_5FeCl^+** are within the typical range for high-spin iron(III) in an octahedral ligand field and resemble the parameters of the other FePOV−alkoxide clusters (Table 4, vide supra).[35] Taking into consideration the 3+ oxidation state of the iron center in complex **5-V_5FeCl^+** and the IR and electronic absorption spectra described above, the chemical oxidation of complex **1-V_5FeX** must occur through the removal of an electron from one

DOI: 10.1021/acs.inorgchem.7b00650
Inorg. Chem. 2017, 56, 7065−7080

of the three vanadium(IV) centers of the POV−alkoxide metalloligand. The formation of **5-V_5FeCl$^+$** indicates the ability of the POV−alkoxide metalloligand to serve as a redox-active reservoir by providing electron density for an oxidation process to occur, resulting in the formation of an Fe−Cl bond. Future work will focus on the development of the reactivity of this platform toward small-molecule activation.

Analysis of Electron Delocalization in FePOV−Alkoxide Clusters. Traditionally, delocalization of the electron density across mixed-valent multimetallic transition-metal complexes can be divided into three categories according to Robin and Day classifications.[53] On the basis of the measurement of the open-circuit potential of **1-V_5FeOClO$_3$** (ca. −0.48 V vs Fc$^+$/Fc) and the previously discussed spectroscopic analysis for the family of FePOV−alkoxide complexes, the redox events observed in the cyclic voltammogram of the FePOV−alkoxide cluster are assigned as $V^{IV}_2V^{V}_3Fe^{III}/V^{IV}_3V^{V}_2Fe^{III}$ ($E_{1/2}$ = +0.14 V), $V^{IV}_3V^{V}_2Fe^{III}/V^{IV}_4V^{V}_1Fe^{III}$ ($E_{1/2}$ = −0.49 V), $V^{IV}_4V^{V}_1Fe^{III}/V^{IV}_5Fe^{III}$ ($E_{1/2}$ = −1.10 V), and $V^{IV}_5Fe^{III}/V^{III}V^{IV}_4Fe^{III}$ ($E_{1/2}$ = −1.60 V) (Figure 1 and Table 1). The large separations between successive one-electron redox events demonstrate the stability of each redox isomer, suggesting a high degree of electron delocalization across the cluster core.[66] The $\Delta E_{1/2}$ values observed for **1-V_5FeOClO$_3$** are similar to those of its homometallic analogue, resulting in a similar range of comproportionation constants between the two series of clusters (K_c = 2.09 × 10^8−5.28 × 10^{10}, RT ln K_c = $nF[\Delta E_{p1} - \Delta E_{p2}]$).[67] The order of magnitude of the experimentally determined K_c values is well established as a good reflection of the extent of electron delocalization within mixed-valent species.[59,68] Complexes with K_c values greater than 10^6 are typically described as systems with significant electron delocalization.

It is important to note that electrochemically determined comproportionation constants may be influenced by the solvent and electrolyte. As such, further evidence for electron delocalization across the cluster core can be extracted from the earlier described spectroscopic characterization of complexes **1-V_5FeOClO$_3$**, **2-V_5Fe**, **3-V_5Fe**, **4-K_2V_5Fe**, and **5-V_5FeCl$^+$**. In the IR spectra of the FePOV−alkoxide clusters, the characteristic band associated with V=O$_t$ is observed as a single absorption, as opposed to resolved features associated with distinct V^V=O$_t$ and V^{IV}=O$_t$ stretching. As such, electron delocalization between vanadium centers within the cluster core occurs at a rate faster than the time scale of IR radiation (10^{-13}−10^{-14} s). In contrast, the electron absorption spectra acquired on the basis of a shorter time scale (10^{-15} s) revealed evidence of localized electron density. In the spectra of complexes **3-KV_5Fe** and **4-K_2V_5Fe**, which do not contain vanadium(V) centers, an absorption band at ∼580 nm was observed. This band is assigned to a $d_{xy}(V^{IV}) \rightarrow d_{x^2-y^2}(V^{IV})$ excitation localized on a single vanadium(IV) center. Although very weak, a similar feature can be observed in the mixed-valent clusters **1-V_5FeOClO$_3$**, **2-V_5Fe**, and **5-V_5FeCl$^+$** (∼680 nm). As pointed out by Hartl and co-workers, such an absorption band cannot be observed in a mixed-valent hexavanadate cluster unless the valence electrons are localized within the time scale of the electron absorption measurement.[43] These observations support conclusions drawn from the electrochemical analysis and comproportionation constants; FePOV−alkoxide clusters can be defined as Robin and Day class II compounds in analogy to their hexavanadate congeners.

CONCLUSION

Herein, we have described the synthesis and systematic investigation of the redox properties of a unique series of mixed-valent FePOV−alkoxide clusters. For example, **1-V_5FeOClO$_3$** was reduced by one electron to form **2-V_5Fe**, which, in turn, could be reduced sequentially to make **3-V_5Fe** and then **4-K_2V_5Fe**. The synthetic results are consistent with cyclic voltammetry experiments that show that **1-V_5FeOClO$_3$** can undergo a series of four reversible one-electron redox events to generate five structurally analogous clusters differing only by their oxidation state. These results demonstrate the ability of the metalloligand to function as an electron reservoir. Mössbauer spectroscopy and XAS confirm retention of the iron(III) oxidation state, while IR and electronic absorption spectroscopies highlight changes in the electronic structure of the POV−alkoxide cluster consistent with reduction. Collectively, these spectroscopic results indicate that sequential redox transformations occur across the highly delocalized POV−alkoxide cluster. Formal charge distributions can be assigned for the POV−alkoxide cluster upon reduction, most notably yielding a fully reduced compound containing a rare vanadium(III) ion. Considering the Mössbauer and Fe K-edge XANES spectra [which suggested that iron(III) is present in each V_5Fe complex] alongside the UV−vis, IR, and magnetic susceptibility data for complex **4-K_2V_5Fe**, our results suggest that reduction generates a vanadium(III) ion within the core.

The synthetic and spectroscopic studies summarized in this work constitute a new class of redox-active ligands. These results indicate that electron delocalization occurs across a reducible metal oxide framework. These metal oxide metalloligands offer an intriguing alternative to traditional organic redox-active ligands, given the established ability for the POV−alkoxide cluster to store four reducing equivalents for the heterometal. Additionally, these multimetallic cluster complexes present new opportunities for exploiting distinct iron and vanadium coordination chemistry. Ongoing efforts in our laboratory are focused on developing an understanding of the reactivity of the family of FePOV−alkoxide cluster complexes for multielectron activation of small molecules.

EXPERIMENTAL SECTION

General Considerations. All manipulations were carried out in the absence of water and oxygen in a UniLab MBraun inert-atmosphere glovebox under a dinitrogen atmosphere. Glassware was oven-dried for a minimum of 4 h and cooled in an evacuated antechamber prior to use in the drybox. Unless otherwise noted, solvents were dried and deoxygenated on a Glass Contour System (Pure Process Technology, LLC) and stored over activated 3 Å molecular sieves purchased from Fisher Scientific. Celite 545 (J. T. Baker) was dried in a Schlenk flask for 14 h at 150 °C under vacuum prior to use. KC_8 (potassium graphite) was prepared by a literature procedure.[69] Silver trifluoromethanesulfonate (AgOTf), silver perchlorate ($AgClO_4$), and tungsten(VI) chloride (WCl_6) were purchased from Sigma-Aldrich and used as received. 4,7,13,16,21,24-Hexaoxa-1,10-diazabicyclo[8.8.8]hexacosane (2,2,2-cryptand) was purchased from Acros through Fisher Scientific and dried overnight under vacuum prior to use. 1,4,7,10,13,16-Hexaoxacyclooctadecane (18-crown-6) was purchased from Alfa Aesar through VWR and recrystallized from dry acetonitrile prior to use. Control molecules for XAS experiments, $[Fe^{II}(MeCN)(TMC)](BF_4)_2$ (TMC = 1,4,8,11-tetramethyl-1,4,8,11-tetraazacyclotetradecane), and ferrous, Fe^{III}(salen)Cl [salen = *N*,*N*′-bis(salicylidene)ethylenediamine], were synthesized according to literature procedures.[38]

^{1}H NMR spectra were recorded at 500 and 400 MHz on Bruker DPX-500 and Bruker DPX-400 MHz spectrometers locked on the

DOI: 10.1021/acs.inorgchem.7b00650
Inorg. Chem. 2017, 56, 7065−7080

signal of deuterated solvents. All chemical shifts were reported relative to the peak of a residual ^{1}H signal in deuterated solvents. $CDCl_3$ and THF-d_8 were purchased from Cambridge Isotope Laboratories, degassed by three freeze−pump−thaw cycles, and stored over activated 3 Å molecular sieves. IR [FT-IR (ATR)] spectra of complexes were recorded on a Shimadzu IR Affinity-1 Fourier transform infrared spectrophotometer and are reported in wavenumbers (cm^{-1}). Electronic absorption measurements were recorded at room temperature in anhydrous acetonitrile in a sealed 1 cm quartz cuvette with an Agilent Cary 60 UV−vis spectrophotometer. Mass spectrometry analyses were performed on a Thermo LTQ Velos liquid chromatograph/mass spectrometer equipped with an electrospray probe operating in positive-ion mode (ESI+) with an ion-trap mass analyzer. Direct injection analysis was employed in all cases with a sample solution in acetonitrile. Single crystals were mounted on the tip of a thin glass optical fiber (goniometer head) and mounted on a Bruker SMART APEX II CCD platform diffractometer for a data collection at 100.0(5) K. The structures were solved using *SHELXT-2014/5*[70] and refined using *SHELXL-2014/7*.[71] Elemental analyses were performed on a PerkinElmer 2400 series II analyzer at the CENTC Elemental Analysis Facility, University of Rochester.

Cyclic voltammetry experiments were recorded with a CH Instruments Inc. 410c time-resolved electrochemical quartz crystal microbalance. All measurements were performed in a three-electrode cell configuration system that consisted of a glassy carbon (⌀ = 3.0 mm) working electrode, a platinum wire counter electrode, and an Ag/AgCl wire reference electrode. All electrochemical measurements were performed at room temperature in a dinitrogen-filled glovebox. A 0.1 M ^{n}Bu$_4$NPF$_6$ solution in dry dicholromethane was used as the electrolyte solution. All redox events were referenced against a ferrocenium/ferrocene (Fc^+/Fc) redox couple.

Fe K-Edge XAFS Measurements. All Fe K-edge XAS data were obtained at the Stanford Synchrotron Radiation Lightsource (SSRL) and Advanced Photon Source (APS). At SSRL, measurements were made under dedicated operating conditions (3.0 GeV, 5%, 500 mA) on end station 11-2. This beamline was equipped with a 26 pole and a 2.0 T wiggler. Using a liquid-nitrogen-cooled double-crystal Si[220] monochromator and employing collimating and focusing mirrors, a single energy was selected from the incident white beam. The crystals were run detuned by 60% to remove higher harmonics from the monochromatic light. Vertical acceptance was controlled by slits positioned before the monochromator. Solid-state XAFS samples were prepared in a dinitrogen-filled glovebox. The analyte was prepared by finely grinding the sample (ca. 5−20 mg) with anhydrous boron nitride (35−45 mg) for 2 min in polystyrene canisters with plexiglass pestles using a Wig-L-Bug grinder to obtain a homogeneous fine powder. Samples were loaded into the slot of an aluminum holder equipped with Kapton windows (1 miL). The samples were brought out of the glovebox, immediately submerged in liquid nitrogen, and transferred to a liquid-helium cryostat on beamline 11-2. The cryostat was attached to the beamline 11-2 XAFS rail. The rail was equipped with three ionization chambers, through which nitrogen gas was continually flowed. One chamber was positioned before the sample holder, to monitor the incident radiation (I_0, 10 cm). The second chamber was positioned after the sample holder, such that the sample transmission (I_1, 30 cm) could be evaluated against I_0, while a third chamber (I_2, 30 cm) was positioned downstream from I_1 so that XANES of a calibration foil could be measured in situ during the XAFS experiments against I_1. Samples were measured exclusively in transmission mode at 85 K. The energy calibration was monitored from experiment to experiment by measuring the XAS spectrum of an europium foil in situ (6977 eV), and the final calibration was made against the first preedge maximum of Fe^{III}(salen)Cl (7112.91 eV). The validity of the calibration was confirmed against [Fe^{II}(MeCN)TMC]-$(BF_4)_2$ (7111.52 eV).

Measurements at the APS were made at the MRCAT Sector 10 ID beamline. This Experimental Section contains a cryo-cooled air-bearing goniometer that results in very high stiffness due to no contact points and a frictionless design. The direct-drive high-torque motor moves a solid shaft with a magnetic field applied to ferrofluids. Motion is encoded externally with a ring encoder, combined with a perfectly balanced crystal cage for both crystals, which allows for quick EXAFS measurements at up to 30°/s Because there are no gear−gear contacts, no mechanical hysteresis is observed, allowing for forward and reverse scanning and reducing the wait time between scans. This beamline uses a double-crystal Si[111/311] monochromator and employs a flat rhodium stripe on SiO_2 focusing and a harmonic rejection mirrror [full width at half-maximum (fwhm) beam spot size = 1.1 × 0.5 mm]. Solid-state XAS samples were prepared in a dinitrogen-filled glovebox. The analyte was prepared by finely grinding the sample (ca. 10−20 mg) for 2 min in polystyrene canisters with plexiglass pestles using a Wig-L-Bug grinder to obtain a homogeneous fine powder. Samples were painted onto the single-sided Kapton (1 mil). The tape was folded 12 times. The tape was placed within a slot of an aluminum holder whose dimensions were 5 × 20 × 1 mm. The holder was equipped with Kapton windows (1 miL) that were sealed with an indium wire gasket. This holder is well established as providing robust exclusion of air and moisture. The sample holder was placed on a rail at the beamline that was equipped with three ionization chambers each with 20-cm-long aluminum ionization plates, through which nitrogen gas was continually flowed. One chamber was positioned before the cryostat to monitor the incident radiation (I_0). The second chamber was positioned after the cryostat so that the sample transmission (I_1) could be evaluated against I_0 and so that the absorption coefficient (μ) could be calculated as $\ln(I_0/I_1)$. The third chamber (I_2) was positioned downstream from I_1 so that the XAFS of a calibration foil could be measured against I_1. Spectra were collected in fluorescence mode using a Lytle detector filled with argon and equipped with a manganese (3) filter and solar slits. Samples were calibrated to the energy of the first inflection point of the K-edge of an iron foil (7111.2 eV), whose spectrum was measured in situ in transmission mode.

Fe K-edge XAS Data Analysis. Data manipulation and analysis was conducted as previously described by Solomon and co-workers.[36] Data were analyzed by fitting a line to the preedge region, which was subsequently subtracted from the experimental data to eliminate the background of the spectrum. The data were normalized by fitting a first-order polynomial to the postedge region of the spectrum and setting the edge jump at 7126 eV to an intensity of 1.0. This normalization procedure gave spectra normalized to a single iron atom or Fe−O bond. A deconvoluted model for the Fe K-edge XAS data was obtained using a modified version of *EDG_FIT*[72] in *IGOR 6.0*. The preedge regions were best modeled by a symmetry-constrained pseudo-Voigt function. The approximate peak positions were determined using first and second derivatives of each spectrum. The edge regions were modeled with pseudo-Voigt functions (for the edge peak). The areas under the preedge peaks (hereafter defined as the intensity) are equal to the fwhm × peak height. Spectra were reproduced 20 times during experimental times at the APS and in duplicate at SSRL. The EXAFS spectra were fit using Athena and Artemis using atomic coordinates from **1-V_5FeOClO$_3$** and **4-K_2V_5Fe** using the FEFF8 platform.[34]

Mössbauer Spectroscopy Measurements and Analysis. All samples for ^{57}Fe Mössbauer spectroscopy were run as isolated solid samples made from natural abundance iron. All samples were prepared in an inert-atmosphere glovebox equipped with a liquid-nitrogen fill port. This enables freezing of the samples to 77 K within the glovebox. Samples were loaded into a Delrin Mössbauer cup for measurements and loaded under liquid nitrogen. ^{57}Fe Mössbauer measurements were performed using a SEE Co. MS4 Mössbauer spectrometer integrated with a Janis SVT-400T He/N_2 cryostat for measurements at 5 and 80 K. Isomer shifts were determined relative to α-iron at 298 K. All Mössbauer spectra were fit using the program *WMoss* (SEE Co.).

Magnetic Susceptibility Measurements. Magnetic susceptibility data were collected using a Quantum Design MPMS XL SQUID magnetometer. Plots that contain the susceptibility data for the individual species can be found in Figure S20. All sample preparations were performed inside a dinitrogen-filled glovebox (MBRAUN Labmaster 130). Powdered microcrystalline samples were loaded into polyethylene bags, sealed in the glovebox, inserted into a straw, and transported to the magnetometer under dinitrogen. Ferromagnetic

DOI: 10.1021/acs.inorgchem.7b00650
Inorg. Chem. 2017, 56, 7065−7080

impurities were probed through a variable-field analysis (0−10 kOe) of the magnetization at 100 K: no curvature was observed in the *M* versus *H* plot (Figure S21), indicating no obvious ferromagnetic impurities present in the samples measured. Magnetic susceptibility data were collected at temperatures ranging from 2 to 300 K. Magnetization measurements were collected at 1.8 K at applied fields ranging from 0 to 50 kOe. Data were corrected for the diamagnetic contributions of the sample holder and bag by subtracting empty containers; corrections for the sample were calculated from Pascal's constants.[73]

*Synthesis of $(VO)_5O(OCH_3)_{12}Fe(ClO_4)$ (**1-V_5FeOClO$_3$**).* **Method A**: Complex **1-V_5FeOClO$_3$** was prepared in a manner similar to that reported for the synthesis of **1-V_5FeOTf**. In the glovebox, $VO(OCH_3)_3$ (0.360 g, 2.25 mmol), $FeBr_2$ (0.162 g, 0.75 mmol), and toluene (18 mL) were placed in four 48 mL heavy-walled pressure vessels, which were then taken out of the glovebox and heated in an oil bath at 85 °C for 110 h with stirring. Dark-brown-green suspensions were eventually obtained, united, and filtered over a bed of Celite (1.0 cm) on a medium-porosity glass frit. The solvent from the resulting dark-green solution was removed under reduced pressure. To the solid residue was added $AgClO_4$ (0.486 g, 2.35 mmol) and MeCN (120 mL). The reaction mixture was stirred vigorously for 2 h, after which the solution was filtered over a bed of Celite (1 cm) and the solvent was removed under reduced pressure. Toluene was then used to extract the solid residue, separating the product from AgBr and excess $AgClO_4$. Removal of volatiles under reduced pressure yields **1-V_5FeOClO$_3$** as a green-yellow powder [1.075 g, 1.22 mmol, 68% based on $VO(OCH_3)_3$]. X-ray-quality crystals were grown from the slow diffusion of *n*-hexane into a concentrated dibutyl ether solution of **1-V_5FeOClO$_3$**. ^{1}H NMR (500 MHz, THF-d_8): δ 25.25 (s, J = 530 Hz), 11.99 (s, J = 708 Hz). FT-IR (ATR, cm^{-1}): 2926 (C−H), 2822 (C−H), 1175 (Cl═O), 1007 (O−CH_3), 979 (V═O). UV−vis [CH_3CN; λ, nm (ε, M^{-1} cm^{-1})]: 378 (1.28×10^4), 992 (8.01×10^2). ESI-MS(+): m/z 778.93 (100%, V_5Fe^+), 819.81 (15%, $V_5Fe^+ + CH_3CN$). Elem anal. Calcd for $C_{12}H_{36}O_{22}V_5FeCl$ (MW = 878.41 g mol^{-1}): C, 16.41; H, 4.13. Found: C, 16.81; H, 3.75.

Method B: In the glovebox, a 20 mL scintillation vial was charged with **2-V_5Fe** (0.040 g, 0.051 mmol), $AgClO_4$ (0.011 g, 0.052 mmol), and 4 mL of THF. The reaction mixture was stirred vigorously for 2 h, during which a brown-yellow precipitate formed. The suspension was filtered, and the solvent was removed under reduced pressure. The solid residue was washed with pentane (5 mL × 3) and extracted with toluene. Removal of volatiles resulted in the isolation of **1-V_5FeOClO$_3$** as a dark-green powder (0.034 g, 0.039, 77%). ^{1}H NMR and FT-IR spectra of the product are identical with that observed for the synthesis of **1-V_5FeOClO$_3$** via method A.

Method C: In the glovebox, a 20 mL scintillation vial was charged with **4-K_2V_5Fe** (0.056 g, 0.065 mmol), $AgClO_4$ (0.039 g, 0.187 mmol), and 4 mL of THF. The reaction mixture was stirred vigorously for 2 h. During the course of the reaction, a large amount of a brown-yellow precipitate formed. The suspension was filtered, resulting in a green-yellow solution. The solvent was removed under reduced pressure. The solid residue was washed with pentane (5 mL × 3) and extracted by toluene. Removal of toluene under vacuum resulted in the isolation of **1-V_5FeOClO$_3$** as a dark-green powder (0.033 g, 0.038 mmol, 57%). ^{1}H NMR and FT-IR spectra of the product are identical with that observed for the synthesis of **1-V_5FeOClO$_3$** via method A.

*Synthesis of $(VO)_5O(OCH_3)_{12}Fe$ (**2-V_5Fe**).* **Method A**: In the glovebox, a 250 mL Erlenmeyer flask was charged with **1-V_5FeOClO$_3$** (1.760 g, 2.00 mmol) and 120 mL of THF. KC_8 (0.292 g, 2.160 mmol) was added slowly to the solution with stirring. The reaction mixture was subsequently stirred vigorously for 1.5 h, after which the solution was filtered over a bed of Celite (1 cm). The solvent was removed under reduced pressure. The solid residue was extracted by toluene. Volatiles were removed under vacuum to yield **2-V_5Fe** as a dark-green powder (1.099 g, 1.41 mmol, 70%). ^{1}H NMR (500 MHz, THF-d_8) δ 23.93 (s, J = 820 Hz), 13.05 (s, J = 906 Hz). FT-IR (ATR, cm^{-1}): 2920 (C−H), 2816 (C−H), 1018 (O−CH_3), 972 (V═O). UV−vis [CH_3CN; λ, nm (ε, M^{-1} cm^{-1})]: 394 (5.20×10^3), 982 (4.83×10^2). Elem anal. Calcd for $C_{12}H_{36}O_{18}V_5Fe$ (MW = 778.95 g mol^{-1}): C, 18.50; H, 4.66. Found: C, 18.36; H, 4.68.

Method B: In the glovebox, a 20 mL scintillation vial was charged with **3-KV_5Fe** (0.041 g, 0.050 mmol), $AgClO_4$ (0.010 g, 0.050 mmol), and 4 mL of CH_3CN. The reaction mixture was stirred vigorously for 2 h. During the course of the reaction, a brown-yellow precipitate formed. The suspension was filtered, resulting in a dark-green solution. The solvent was removed under reduced pressure, and the remaining dark-green residue was extracted by toluene. The removal of toluene under vacuum resulted in the isolation of **2-V_5Fe** as a dark-green powder (0.029 g, 0.037 mmol, 74%). ^{1}H NMR and FT-IR spectra of the product are identical with that observed for **2-V_5Fe** generated through method A.

*Synthesis of $K[(VO)_5O(OCH_3)_{12}Fe]$ (**3-KV_5Fe**).* **Method A**: In the glovebox, a 20 mL scintillation vial was charged with **2-V_5Fe** (0.162 g, 0.208 mmol), KC_8 (30 mg, 0.222 mmol), and 20 mL of THF. A distinct color change from deep green to blue-green was observed within the first 5 min of the reaction; however, the mixture was left to stir for an additional 1.5 h to ensure completion. The mixture was filtered over a bed of Celite (1 cm), yielding a dark-green-blue solution. Volatiles were removed under reduced pressure to yield **3-KV_5Fe** as a dark-green-blue powder (154 mg, 0.188 mmol, 91%). ^{1}H NMR (500 MHz, THF-d_8) δ 23.75 (s, J = 1082 Hz). FT-IR (ATR, cm^{-1}): 2916 (C−H), 2812 (C−H), 1038 (O−CH_3), 943 (V═O). UV−vis [CH_3CN; λ, nm (ε, M^{-1} cm^{-1})]: 298 (7.35×10^3), 590 (3.25×10^2). Elem anal. Calcd for $C_{12}H_{36}O_{18}V_5FeK$ (MW = 818.05 g mol^{-1}): C, 17.62; H, 4.44. Found: C, 17.51; H, 4.07.

Method B: In the glovebox, a 20 mL scintillation vial was charged with **4-K_2V_5Fe** (55.1 g, 0.064 mmol), $AgClO_4$ (13.3 mg, 0.064 mmol), and 4 mL of CH_3CN. The reaction mixture was stirred vigorously for 2 h, during which a brown-yellow precipitate formed. The suspension was filtered, resulting in a green-blue solution. The solvent was removed under reduced pressure. The solid residue was washed with toluene (5 mL × 3) and diethyl ether (5 mL × 3) and then extracted by THF. Volatiles were removed under reduced pressure to yield **3-KV_5Fe** as a dark-green-blue powder (0.044 g, 0.054 mmol, 83%). ^{1}H NMR and FT-IR spectra collected for the product are identical with that observed for method A.

*Synthesis of $K_2[(VO)_5O(OCH_3)_{12}Fe]$ (**4-K_2V_5Fe**).* **Method A**: In the glovebox, a 20 mL scintillation vial was charged with **3-KV_5Fe** (0.164 g, 0.200 mmol), KC_8 (0.030 g, 0.222 mmol), and 20 mL of THF. The color of the mixture changed from blue-green to deep purple within 5 min. The reaction mixture was stirred vigorously for 1.5 h to ensure completion, after which the mixture was filtered over a bed of Celite (1 cm). The solvent was removed under reduced pressure to yield **4-K_2V_5Fe** as a purple-blue powder (0.135 g, 0.158 mmol mmol 79%). Crystals suitable for X-ray analysis were grown by the slow diffusion of pentane into a concentrated THF solution of **4-K_2V_5Fe** in the presence of 2 equiv of 2,2,2-crpytand. ^{1}H NMR (400 MHz, THF-d_8): δ 25.03 (s, 2078 Hz). FT-IR (ATR, cm^{-1}): 2895 (C−H), 2808 (C−H), 1047 (O−CH_3), 939 (V═O). UV−vis [CH_3CN; λ, nm (ε, M^{-1} cm^{-1})]: 300 (8.52×10^3), 548 (3.56×10^2). Elem anal. Calcd for $C_{12}H_{36}O_{18}V_5FeK_2$ (MW = 857.15 g mol^{-1}): C, 16.81; H, 4.23. Found: C, 16.93; H, 4.13. Elem anal. Calcd for $C_{48}H_{108}N_4O_{30}V_5FeK_2$ [(K-crypt)$_2V_5$Fe] (MW = 1610.12 g mol^{-1}): C, 35.81; H, 6.76; N, 3.48. Found: C, 36.10; H, 6.58; N, 3.10.

Method B: In the glovebox, a 250 mL Erlenmeyer flask was charged with **1-V_5FeOClO$_3$** (1.340 g, 1.525 mmol), KC_8 (0.670 g, 4.956 mmol), and 120 mL of THF. The reaction mixture was stirred vigorously for 1.5 h, during which the color of the suspension changed from dark green to deep purple-blue. The solution was filtered over a bed of Celite (1 cm), and the solvent was removed under reduced pressure to yield **4-K_2V_5Fe** as a purple-blue powder (0.770 g, 0.898 mmol, 59%). ^{1}H NMR and FT-IR spectra of the product are identical with that observed for the synthesis of **4-K_2V_5Fe** via method A.

*Synthesis of $(VO)_5O(OCH_3)_{12}Fe(OCN)$ (**1-V_5FeOCN**).* Complex **1-V_5FeOCN** was prepared in a manner similar to that reported for the syntheses of **1-V_5FeOTf** and **1-V_5FeOClO$_3$**. A 20 mL scintillation vial was charged with **1-V_5FeBr** (0.200 g, 0.23 mmol), AgOCN (0.103 g, 0.69 mmol), and 20 mL of dichloromethane (DCM). The mixture was stirred for 2 h at room temperature, after which the solvent was removed under reduced pressure. Toluene was used to extract the

DOI: 10.1021/acs.inorgchem.7b00650
Inorg. Chem. 2017, 56, 7065−7080

solid residue, separating the product from AgBr and residual AgOCN. After the removal of volatiles under reduced pressure, the solid residue was extracted by pentane (10 mL × 3). The extraction was united and concentrated to about one-third of the original volume and left at −30 °C for 2 days to obtain **1-V_5FeOCN** as a dark-green solid (0.128 g, 0.16 mmol, 68%). ^{1}H NMR (400 MHz, $CDCl_3$): δ 24.69 (s, 500 Hz), 12.12 (s, 768 Hz). FT-IR (ATR, cm^{-1}): 2924 (C−H), 2818 (C−H), 2197 (C≡N), 1016 (O−CH_3), 976 (V═O). UV−vis [CH_3CN; λ, nm (ε, M^{-1} cm^{-1})]: 320 (2.16×10^4), 394 (9.85×10^3), 986 (1.08×10^3). ESI-MS(+): m/z 820.87 (100%, V_5FeOCN). Elem anal. Calcd for $C_{13}H_{36}NO_{19}V_5Fe$ (MW = 820.97 g mol^{-1}): C, 19.02; H, 4.42; N, 1.71. Found: C, 19.31; H, 4.07; N, 1.91.

Synthesis of [(VO)$_5$O(OCH$_3$)$_{12}$FeCl](FeCl$_4$)·THF (5-[V_5FeCl][FeCl$_4$]). In the glovebox, a 20 mL scintillation vial was charged with **1-V_5FeOTf** (0.186 g, 0.200 mmol), WCl_6 (0.027 g, 0.067 mmol), and 20 mL of DCM. The reaction mixture was stirred vigorously for 30 min, after which the solvent was removed under reduced pressure and the solid residue was extracted by THF (5 mL × 2). The extraction was combined and concentrated to one-third of its original volume and stored at −30 °C for 3 days. A small amount of dark-green thin-plate crystals of **5-[V_5FeCl]$^+$**, suitable for X-ray crystallography, was obtained (0.032 g, 0.030 mmol, 15%). ^{1}H NMR (400 MHz, THF-d_8): δ 23.98 (s, br, J = 536 Hz), 12.47 (s, br, J = 660 Hz). FT-IR (ATR, cm^{-1}): 2932 (C−H), 2828 (C−H), 986 (V═O). UV−vis [CH_3CN; λ, nm (ε, M^{-1} cm^{-1})]: 302 (1.96×10^4), 370 (1.46×10^4), 992 (6.58×10^2). ESI-MS(+): m/z 814.22 (100%), 815.93 (27%) (V_5FeCl^+). Elem anal. Calcd for $C_{16}H_{44}O_{19}V_5Fe_2Cl_5$ (MW = 1084.17 g mol^{-1}): C, 17.73; H, 4.09. Found: C, 17.88; H, 4.06.

Synthesis of [(VO)$_5$O(OCH$_3$)$_{12}$FeCl](SO$_3$CF$_3$) (5-[V_5FeCl]OTf). In the glovebox, a 20 mL scintillation vial was charged with **1-V_5FeOTf** (0.186 g, 0.200 mmol), WCl_6 (0.027 g, 0.067 mmol), and 20 mL of DCM. The reaction mixture was stirred vigorously for 30 min, after which the solvent was removed under reduced pressure. The solid residue was washed with *n*-hexane several times until the hexane extraction turned colorless. The solid residue was then extracted by toluene, and the removal of volatiles yielded **5-[V_5FeCl]$^+$OTf** as a dark-yellow-green solid (0.082 g, 0.081 mmol, 43%). ^{1}H NMR (500 MHz, THF-d_8): δ 24.21 (s, J = 325 Hz), 12.06 (s, J = 565 Hz). FT-IR (ATR, cm^{-1}): 2932 (C−H), 2828 (C−H), 986 (V═O). UV−vis [CH_3CN; λ, nm (ε, M^{-1} cm^{-1})]: 302 (2.29×10^4), 370 (1.46×10^4), 988 (6.91×10^2). ESI-MS(+): m/z 814.22 (100%), 815.93 (27%) (V_5FeCl^+). Elem anal. Calcd for $C_{13}H_{36}O_{21}V_5FeClSF_3$ (MW = 963.48 g mol^{-1}): C, 16.21; H, 3.77. Found: C, 16.48; H, 3.57.

The CCDC has the supplementary crystallographic data for this paper: **1-V_5FeOClO$_3$**, 1504756; **4-K_2V_5Fe**, 1504755; **5-V_5FeCl**, 1504757.

■ ASSOCIATED CONTENT

Supporting Information

The Supporting Information is available free of charge on the ACS Publications website at DOI: 10.1021/acs.inorgchem.7b00650.

Spectral data for complexes **1-V_5FeOClO$_3$**, **1-V_5FeOCN**, **2-V_5Fe**, **3-KV_5Fe**, **4-K_2V_5Fe**, and **5-V_5FeCl$^+$** and general considerations pertaining to spectroscopic data collection (PDF)

Accession Codes

CCDC 1504755−1504757 contains the supplementary crystallographic data for this paper. These data can be obtained free of charge via www.ccdc.cam.ac.uk/data_request/cif, or by emailing data_request@ccdc.cam.ac.uk, or by contacting The Cambridge Crystallographic Data Centre, 12, Union Road, Cambridge CB2 1EZ, UK; fax: +44 1223 336033.

■ AUTHOR INFORMATION

Corresponding Author

*E-mail: matson@chem.rochester.edu.

ORCID

William W. Brennessel: 0000-0001-5461-1825
Maryline G. Ferrier: 0000-0003-0081-279X
Samantha K. Cary: 0000-0003-0398-7106
Michael L. Neidig: 0000-0002-2300-3867
Ellen M. Matson: 0000-0003-3753-8288

Notes

The authors declare no competing financial interest.

■ ACKNOWLEDGMENTS

The authors acknowledge Lauren E. Van Gelder for helpful discussions during the writing of this manuscript. This research was funded by the National Science Foundation through Grants CHE-1653195 (to F.L., M.G.H., and E.M.M.), CHE-1454370 (to S.H.C. and M.L.N.), and CHE-1363274 (to R.F.H. and M.P.S.). F.L., M.G.H., and E.M.M. also acknowledge support from the University of Rochester for this work. XAFS studies were supported by the Division of Chemical Sciences, Geosciences, and Biosciences, Office of Basic Energy Sciences, U.S. Department of Energy (DOE; to S.A.K. and J.S.L.-P.). Portions of this work were supported by postdoctoral fellowships from the Glenn T. Seaborg Institute (to M.G.F. and B.W.S.) and the LANL Marie Curie Named Fellowship (to S.K.C.). Los Alamos National Laboratory is operated by Los Alamos National Security, LLC, for the National Nuclear Security Administration of U.S. DOE (Contract DE-AC52-06NA25396). Use of the SSRL, SLAC National Accelerator Laboratory, was supported by the U.S. DOE, Office of Science, Office of Basic Energy Sciences, under Contract DE-AC02-76SF00515. The SSRL Structural Molecular Biology Program is supported by the U.S. DOE, Office of Biological and Environmental Research, and by the National Institutes of Health, National Institute of General Medical Sciences (including P41GM103393). MRCAT operations are supported by the U.S. DOE and the MRCAT member institutions. This research used resources of the APS, a U.S. DOE, Office of Science User Facility, operated for the U.S. DOE, Office of Science, by Argonne National Laboratory under Contract DE-AC02-06CH11357.

■ REFERENCES

(1) Hartwig, J. *Organotransition Metal Chemistry: From Bonding to Catalysis*; University Science Books: Sausilito, CA, 2009.
(2) Crabtee, R. H. *The Organometallic Chemistry of the Transition Metals*, 6th ed.; John Wiley & Sons: New York, 2014.
(3) *Mineral Commodity Summaries 2013*; U.S. Geological Survey: Reton, VA, 2013.
(4) de Meijere, A. Organometallics in Organic Synthesis: Introduction. *Chem. Rev.* **2000**, *100*, 2739−2740.
(5) Buchwald, S. L.; Bolm, C. On the Role of Metal Contaminants in Catalyses with $FeCl_3$. *Angew. Chem., Int. Ed.* **2009**, *48*, 5586−5587.
(6) Lippert, C. A.; Hardcastle, K. I.; Soper, J. D. Harnessing Redox-Active Ligands for Low-Barrier Radical Addition at Oxorhenium Complexes. *Inorg. Chem.* **2011**, *50*, 9864−9878.
(7) Chirik, P. J.; Wieghardt, K. Radical Ligands Confer Nobility on Base-Metal Catalysts. *Science* **2010**, *327*, 794−795.
(8) Parshall, G. W.; Ittel, S. D. *The Applications and Chemistry of Catalysis by SOluble Transition Metal Complexes*, 2nd ed.; Wiley-Interscience: New York, 1992.

DOI: 10.1021/acs.inorgchem.7b00650
Inorg. Chem. 2017, 56, 7065−7080

(9) Luca, O. R.; Crabtree, R. H. Redox-active ligands in catalysis. *Chem. Soc. Rev.* **2013**, *42*, 1440−1459.
(10) Lyaskovskyy, V.; de Bruin, B. Redox Non-Innocent Ligands: Versatile New Tools to Control Catalytic Reactions. *ACS Catal.* **2012**, *2*, 270−279.
(11) Schmidt, V. A.; Hoyt, J. M.; Margulieux, G. W.; Chirik, P. J. Cobalt-Catalyzed [2π + 2π] Cycloadditions of Alkenes: Scope, Mechanism, and Elucidation of Electronic Structure of Catalytic Intermediates. *J. Am. Chem. Soc.* **2015**, *137*, 7903−7914.
(12) Bouwkamp, M. W.; Bowman, A. C.; Lobkovsky, E.; Chirik, P. J. Iron-Catalyzed [2π + 2π] Cycloaddition of α,ω-Dienes: The Importance of Redox-Active Supporting Ligands. *J. Am. Chem. Soc.* **2006**, *128*, 13340−13341.
(13) Stubbert, B. D.; Peters, J. C.; Gray, H. B. Rapid Water Reduction to H2 Catalyzed by a Cobalt Bis(iminopyridine) Complex. *J. Am. Chem. Soc.* **2011**, *133*, 18070−18073.
(14) Luca, O. R.; Konezny, S. J.; Blakemore, J. D.; Colosi, D. M.; Saha, S.; Brudvig, G. W.; Batista, V. S.; Crabtree, R. H. A tridentate Ni pincer for aqueous electrocatalytic hydrogen production. *New J. Chem.* **2012**, *36*, 1149−1152.
(15) Lei, H.; Fang, H.; Han, Y.; Lai, W.; Fu, X.; Cao, R. Reactivity and Mechanism Studies of Hydrogen Evolution Catalyzed by Copper Corroles. *ACS Catal.* **2015**, *5*, 5145−5153.
(16) Letko, C. S.; Panetier, J. A.; Head-Gordon, M.; Tilley, T. D. Mechanism of the Electrocatalytic Reduction of Protons with Diaryldithiolene Cobalt Complexes. *J. Am. Chem. Soc.* **2014**, *136*, 9364−9376.
(17) Smith, A. L.; Hardcastle, K. I.; Soper, J. D. Redox-Active Ligand-Mediated Oxidative Addition and Reductive Elimination at Square Planar Cobalt(III): Multielectron Reactions for Cross-Coupling. *J. Am. Chem. Soc.* **2010**, *132*, 14358−14360.
(18) Haneline, M. R.; Heyduk, A. F. C−C Bond-Forming Reductive Elimination from a Zirconium(IV) Redox-Active Ligand Complex. *J. Am. Chem. Soc.* **2006**, *128*, 8410−8411.
(19) Hutin, M.; Rosnes, M. H.; Long, D. L.; Cronin, L. Polyoxometalates: Synthesis and Structure—From Building Blocks to Emergent Materials A2. In *Comprehensive Inorganic Chemistry II*, 2nd ed.; Reedijk, J., Poeppelmeier, K., Eds.; Elsevier: Amsterdam, The Netherlands, 2013; Chapter 2.10, pp 241−269.
(20) Pope, M. T.; Müller, A. Polyoxometalate Chemistry: An Old Field with New Dimensions in Several Disciplines. *Angew. Chem., Int. Ed. Engl.* **1991**, *30*, 34−48.
(21) Pope, M.; Müller, A. *Polyoxometalate Chemistry: From Topology via Self-Assembly to Applications*; Springer: Dordrecht, The Netherlands, 2001.
(22) Tucher, J.; Schlicht, S.; Kollhoff, F.; Streb, C. Photocatalytic reactivity tuning by heterometal and addenda metal variation in Lindqvist polyoxometalates. *Dalton Trans.* **2014**, *43*, 17029−17033.
(23) Dave, M.; Streb, C. Oxidative photoreactivity of mono-transition-metal functionalized lacunary Keggin anions. *Dalton Trans.* **2015**, *44*, 18919−18922.
(24) Kastner, K.; Streb, C. Polyoxometalates in Photocatalysis. In *Chemical Photocatalysis*; König, B., Ed.; De Gruyter: Berlin, Germany, 2013; pp 247−258.
(25) Hill, C. L.; Prosser-McCartha, C. M. Homogeneous catalysis by transition metal oxygen anion clusters. *Coord. Chem. Rev.* **1995**, *143*, 407−455.
(26) Hill, C. L. Progress and challenges in polyoxometalate-based catalysis and catalytic materials chemistry. *J. Mol. Catal. A: Chem.* **2007**, *262*, 2−6.
(27) Lechner, M.; Guttel, R.; Streb, C. Challenges in polyoxometalate-mediated aerobic oxidation catalysis: catalyst development meets reactor design. *Dalton Trans.* **2016**, *45*, 16716−16726.
(28) Li, F.; VanGelder, L. E.; Brennessel, W. W.; Matson, E. M. Self-Assembled, Iron-Functionalized Polyoxovanadate Alkoxide Clusters. *Inorg. Chem.* **2016**, *55*, 7332−7334.
(29) Spandl, J.; Daniel, C.; Brüdgam, I.; Hartl, H. Synthesis and Structural Characterization of Redox-Active Dodecamethoxoheptaoxohexavanadium Clusters. *Angew. Chem., Int. Ed.* **2003**, *42*, 1163−1166.
(30) Daniel, C.; Hartl, H. Neutral and Cationic VIV/VV Mixed-Valence Alkoxo-polyoxovanadium Clusters $[V_6O_7(OR)_{12}]^{n+}$ (R = $-CH_3$, $-C_2H_5$): Structural, Cyclovoltammetric and IR-Spectroscopic Investigations on Mixed Valency in a Hexanuclear Core. *J. Am. Chem. Soc.* **2005**, *127*, 13978−13987.
(31) Bard, A. J.; Faulkner, L. R. *Electrochemical Methods: Fundamentals and Applications*, 2nd ed.; John Wiley & Sons: Hoboken, NJ, 2001.
(32) Lindqvist, I. *Ark. Kemi* **1953**, *5*, 246−250.
(33) Harris, T. D.; Betley, T. A. Multi-Site Reactivity: Reduction of Six Equivalents of Nitrite To Give an $Fe_6(NO)_6$ Cluster with a Dramatically Expanded Octahedral Core. *J. Am. Chem. Soc.* **2011**, *133*, 13852−13855.
(34) Ankudinov, A.; Conradson, S.; Mustre de Leon, J.; Rehr, J. Relativistic XANES calculations of Pu hydrates. *Phys. Rev. B: Condens. Matter Mater. Phys.* **1998**, *57*, 7518−7525.
(35) Gütlich, P.; Bill, E.; Trautwein, A. X. *Mössbauer Spectroscopy and Transition Metal Chemistry*; Springer: Berlin, Germany, 2011.
(36) Solomon, E. I.; Hedman, B.; Hodgson, K. O.; Dey, A.; Szilagyi, R. K. Ligand K-edge X-ray absorption spectroscopy: covalency of ligand−metal bonds. *Coord. Chem. Rev.* **2005**, *249*, 97−129.
(37) Hocking, R. K.; DeBeer George, S.; Raymond, K. N.; Hodgson, K. O.; Hedman, B.; Solomon, E. I. Fe L-Edge X-ray Absorption Spectroscopy Determination of Differential Orbital Covalency of Siderophore Model Compounds: Electronic Structure Contributions to High Stability Constants. *J. Am. Chem. Soc.* **2010**, *132*, 4006−4015.
(38) Westre, T. E.; Kennepohl, P.; DeWitt, J. G.; Hedman, B.; Hodgson, K. O.; Solomon, E. I. A Multiplet Analysis of Fe K-Edge 1s → 3d Pre-Edge Features of Iron Complexes. *J. Am. Chem. Soc.* **1997**, *119*, 6297−6314.
(39) Tondreau, A. M.; Stieber, S. C. E.; Milsmann, C.; Lobkovsky, E.; Weyhermüller, T.; Semproni, S. P.; Chirik, P. J. Oxidation and Reduction of Bis(imino)pyridine Iron Dinitrogen Complexes: Evidence for Formation of a Chelate Trianion. *Inorg. Chem.* **2013**, *52*, 635−646.
(40) Enright, D.; Gambarotta, S.; Yap, G. P. A.; Budzelaar, P. H. M. The Ability of the α,α'-Diiminopyridine Ligand System to Accept Negative Charge: Isolation of Paramagnetic and Diamagnetic Trianions. *Angew. Chem., Int. Ed.* **2002**, *41*, 3873−3876.
(41) Ciccione, J.; Leconte, N.; Luneau, D.; Philouze, C.; Thomas, F. Geometric and Electronic Structures of Nickel(II) Complexes of Redox Noninnocent Tetradentate Phenylenediamine Ligands. *Inorg. Chem.* **2016**, *55*, 649−665.
(42) Chaudhuri, P.; Hess, M.; Müller, J.; Hildenbrand, K.; Bill, E.; Weyhermüller, T.; Wieghardt, K. Aerobic Oxidation of Primary Alcohols (Including Methanol) by Copper(II)− and Zinc(II)−Phenoxyl Radical Catalysts. *J. Am. Chem. Soc.* **1999**, *121*, 9599−9610.
(43) Daniel, C.; Hartl, H. A Mixed-Valence VIV/VV Alkoxo-polyoxovanadium Cluster Series $[V_6O_8(OCH_3)_{11}]^{n\pm}$: Exploring the Influence of a μ-Oxo Ligand in a Spin Frustrated Structure. *J. Am. Chem. Soc.* **2009**, *131*, 5101−5114.
(44) Rocchiccioli-Deltcheff, C.; Thouvenot, R.; Fouassier, M. Vibrational investigations of polyoxometallates. 1. Valence force field of $Mo_6O_{19}^{2-}$ based on total isotopic substitution (oxygen-18, molybdenum-92, molybdenum-100). *Inorg. Chem.* **1982**, *21*, 30−35.
(45) Demadis, K. D.; Hartshorn, C. M.; Meyer, T. J. The Localized-to-Delocalized Transition in Mixed-Valence Chemistry. *Chem. Rev.* **2001**, *101*, 2655−2686.
(46) Sanchez, C.; Livage, J.; Launay, J. P.; Fournier, M.; Jeannin, Y. Electron delocalization in mixed-valence molybdenum polyanions. *J. Am. Chem. Soc.* **1982**, *104* (11), 3194−3202.
(47) Pope, M. *Heteropoly and Isopoly Oxometalates*, 1st ed.; Springer-Verlag: Berlin, Germany, 1983.
(48) Müller, A.; Meyer, J.; Bögge, H.; Stammler, A.; Botar, A. Cis-/Trans-Isomerie bei Bis-(trisalkoxy)-hexavanadaten: cis-$Na_2[V_6O_7(OH)_6\{(OCH_2)_3CCH_2OH\}_2]\cdot 8H_2O$, cis-$(CN_3H_6)_3[V_6O_{13}\{(OCH_2)_3CCH_2OH\}_2]\cdot 4{,}5H_2O$ und trans-$(CN_3H_6)_2[V_6O_{13}\{(OCH_2)_3CCH_2OH\}_2]\cdot H_2O$. *Z. Anorg. Allg. Chem.* **1995**, *621*, 1818−1831.

DOI: 10.1021/acs.inorgchem.7b00650
Inorg. Chem. 2017, 56, 7065−7080

(49) Batchelor, L. J.; Shaw, R.; Markey, S. J.; Helliwell, M.; McInnes, E. J. L. An All-Vanadium(III) Hexametalate Lindqvist Structure and Its Chromium and Iron Analogues. *Chem. - Eur. J.* **2010**, *16*, 5554−5557.
(50) Aronica, C.; Chastanet, G.; Zueva, E.; Borshch, S. A.; Clemente-Juan, J. M.; Luneau, D. A Mixed-Valence Polyoxovanadate(III,IV) Cluster with a Calixarene Cap Exhibiting Ferromagnetic V(III)−V(IV) Interactions. *J. Am. Chem. Soc.* **2008**, *130*, 2365−2371.
(51) Khan, M. I.; Chen, Q.; Zubieta, J.; Goshorn, D. P. Hexavanadium polyoxoalkoxide anion clusters: structures of the mixed-valence species $(Me_3NH)[V^{IV}_5V^{V}O_7(OH)_3\{CH_3C(CH_2O)_3\}_3]$ and of the reduced complex $Na_2[V^{IV}_6O_7\{CH_3CH_2C(CH_2O)_3\}_4]$. *Inorg. Chem.* **1992**, *31*, 1556−1558.
(52) Chen, Q.; Goshorn, D. P.; Scholes, C. P.; Tan, X. L.; Zubieta, J. Coordination compounds of polyoxovanadates with a hexametalate core. Chemical and structural characterization of $[V^{V}_6O_{13}[(OCH_2)_3CR]_2]^{2-}$, $[V^{V}_6O_{11}(OH)_2[(OCH_2)_3CR]_2]$, $[V^{IV}_4V^{V}_2O_9(OH)_4[(OCH_2)_3CR]_2]^{2-}$, and $[V^{IV}_6O_7(OH)_6](OCH_2)_3CR]_2]^{2-}$. *J. Am. Chem. Soc.* **1992**, *114*, 4667−4681.
(53) Robin, M. B.; Day, P. Mixed Valence Chemistry—A Survey and Classification. In *Advances in Inorganic Chemistry and Radiochemistry*; Emeléus, H. J., Sharpe, A. G., Eds.; Academic Press: New York, 1968; Vol. *10*, pp 247−422.
(54) Zueva, E. M.; Herchel, R.; Borshch, S. A.; Govor, E. V.; Sameera, W. M. C.; McDonald, R.; Singleton, J.; Krzystek, J.; Travnicek, Z.; Sanakis, Y.; McGrady, J. E.; Raptis, R. G. Double exchange in a mixed-valent octanuclear iron cluster, $[Fe_8(\mu^4\text{-}O)_4(\mu^4\text{-}Cl\text{-}pz)_{12}Cl_4]$. *Dalton Trans.* **2014**, *43*, 11269−11276.
(55) Barbaro, P.; Bencini, A.; Bertini, I.; Briganti, F.; Midollini, S. The tetranuclear trianion $[Fe_4Te_4(SC_6H_5)_4]^{3-}$: crystal and molecular structure and magnetic properties. *J. Am. Chem. Soc.* **1990**, *112*, 7238−7246.
(56) Zhao, Q.; Harris, T. D.; Betley, T. A. $[(HL)_2Fe_6(NCMe)_m]^{n+}$ (m = 0, 2, 4, 6; n = − 1, 0, 1, 2, 3, 4, 6): An Electron-Transfer Series Featuring Octahedral Fe_6 Clusters Supported by a Hexaamide Ligand Platform. *J. Am. Chem. Soc.* **2011**, *133*, 8293−8306.
(57) Harris, T. D.; Zhao, Q.; Sanchez, R. H.; Betley, T. A. Expanded redox accessibility via ligand substitution in an octahedral Fe_6Br_6 cluster. *Chem. Commun.* **2011**, *47*, 6344−6346.
(58) Sánchez, R. H.; Willis, A. M.; Zheng, S.-L.; Betley, T. A. Synthesis of Well-Defined Bicapped Octahedral Iron Clusters $[(trenL)_2Fe_8(PMe_2Ph)_2]^n$ (n = 0, − 1). *Angew. Chem., Int. Ed.* **2015**, *54*, 12009−12013.
(59) Hernández Sánchez, R.; Zheng, S.-L.; Betley, T. A. Ligand Field Strength Mediates Electron Delocalization in Octahedral $[(HL)_2Fe_6(L')_m]^{n+}$ Clusters. *J. Am. Chem. Soc.* **2015**, *137*, 11126−11143.
(60) Hoffmann, A.; Flörke, U.; Herres-Pawlis, S. Insights into Different Donor Abilities in Bis(pyrazolyl)pyridinylmethane Transition Metal Complexes. *Eur. J. Inorg. Chem.* **2014**, *2014* (13), 2296−2306.
(61) Willans, C. E.; Anderson, K. M.; Junk, P. C.; Barbour, L. J.; Steed, J. W. A small tris(imidazolium) cage forms an N-heterocyclic carbene complex with silver(I). *Chem. Commun.* **2007**, 3634−3636.
(62) Batten, M. P.; Canty, A. J.; Cavell, K. J.; Ruther, T.; Skelton, B. W.; White, A. H. Bis[tris(1-methyl-1H-imidazol-2-yl)phosphine-κ^3N_3]iron(II) tetrachloroferrate(II) methanol tetrasolvate (ca 153 K) and bis[tris(1-methyl-1H-imidazol-2-yl)methanol-κ^3N_3]iron(III) bis-[tetrachloroferrate(III)] chloride (redetermination, ca 153 K). *Acta Crystallogr., Sect. C: Cryst. Struct. Commun.* **2004**, *60*, m311−m313.
(63) Jakonen, M.; Oresmaa, L.; Haukka, M. Solid-State Packing of the Square-Planar $[RhI(H_2bim)(CO)_2]_2[A]$ Complexes (H_2bim = 2,2-biimidazole; [A] = 2[Cl], 2$[RhICl_2(CO)_2]$, $[Fe^{II}Cl_4]$, $[Co^{II}Cl_4]$. *Cryst. Growth Des.* **2007**, *7*, 2620−2626.
(64) Kim, M.; Kim, Y.-U.; Han, J. X-ray crystallographic structure and physical properties of the pentacoordinated $[TPAFeCl]^+$ complex. *Polyhedron* **2007**, *26*, 4003−4008.
(65) Groom, C. R.; Bruno, I. J.; Lightfoot, M. P.; Ward, S. C. The Cambridge Structural Database. *Acta Crystallogr., Sect. B: Struct. Sci., Cryst. Eng. Mater.* **2016**, *72*, 171−179.
(66) Heinze, J. Cyclic Voltammetry—"Electrochemical Spectroscopy". New Analytical Methods. *Angew. Chem., Int. Ed. Engl.* **1984**, *23*, 831−847.
(67) Richardson, D. E.; Taube, H. Determination of E20-E10 in multistep charge transfer by stationary-electrode pulse and cyclic voltammetry: application to binuclear ruthenium ammines. *Inorg. Chem.* **1981**, *20*, 1278−1285.
(68) Ward, M. D. Metal-metal interactions in binuclear complexes exhibiting mixed valency; molecular wires and switches. *Chem. Soc. Rev.* **1995**, *24*, 121−134.
(69) Weitz, I. S.; Rabinovitz, M. The application of C_8K for organic synthesis: reduction of substituted naphthalenes. *J. Chem. Soc., Perkin Trans. 1* **1993**, 117−120.
(70) Sheldrick, G. M. *SHELXT-2014/5*; University of Göttingen: Göttingen, Germany, 2014.
(71) Sheldrick, G. Crystal structure refinement with SHELXL. *Acta Crystallogr., Sect. C: Struct. Chem.* **2015**, *71*, 3−8.
(72) George, G. *ENG_FIT*; TWI: Cambridge, U.K., 2006.
(73) Bain, G. A.; Berry, J. F. Diamagnetic corrections and Pascal's constants. *J. Chem. Educ.* **2008**, *85*, 532−536.

DOI: 10.1021/acs.inorgchem.7b00650
Inorg. Chem. 2017, 56, 7065−7080